Lab on a Chip

CRITICAL REVIEW

View Article Online
View Journal | View Issue

Cite this: *Lab Chip*, 2024, **24**, 1244

Harvesting and manipulating sweat and interstitial fluid in microfluidic devices

Tamoghna Saha , †‡* Sneha Mukherjee, ‡
Michael D. Dickey * and Orlin D. Velev *

Microfluidic devices began to be used to facilitate sweat and interstitial fluid (ISF) sensing in the mid-2010s. Since then, numerous prototypes involving microfluidics have been developed in different form factors for sensing biomarkers found in these fluids under *in vitro*, *ex vivo*, and *in vivo* (on-body) settings. These devices transport and manipulate biofluids using microfluidic channels composed of silicone, polymer, paper, or fiber. Fluid flow transport and sample management can be achieved by controlling the flow rate, surface morphology of the channel, and rate of fluid evaporation. Although many devices have been developed for estimating sweat rate, electrolyte, and metabolite levels, only a handful have been able to proceed beyond laboratory testing and reach the stage of clinical trials and commercialization. To further this technology, this review reports on the utilization of microfluidics towards sweat and ISF management and transport. The review is distinguished from other recent reviews by focusing on microfluidic principles of sweat and ISF generation, transport, extraction, and management. Challenges and prospects are highlighted, with a discussion on how to transition such prototypes towards personalized healthcare monitoring systems.

Received 13th October 2023,
Accepted 22nd December 2023

DOI: 10.1039/d3lc00874f

rsc.li/loc

1. Introduction

This review focuses on the use of microfluidics to harness, transport, and manipulate sweat and interstitial fluid (ISF) in wearable health tracking and diagnostic devices. Such devices offer the promise of improved health outcomes and reduced healthcare costs by providing individuals with continuous (used interchangeably with "real-time", especially when referring to data acquisition in wearable systems) monitoring

Department of Chemical and Biomolecular Engineering, North Carolina State University, Raleigh, NC 27695, USA. E-mail: tsaha@ucsd.edu, mddickey@ncsu.edu, odvelev@ncsu.edu

† Currently: Department of Chemical and Nanoengineering, University of California, San Diego, La Jolla, CA 92093, USA

‡ Equal contribution.

Tamoghna Saha

Tamoghna Saha is currently a postdoctoral scholar in the Department of Nanoengineering at the University of California, San Diego (UCSD) working with Prof. Joseph Wang since Feb. 2022 on sweat/ISF wearables and biofuel cells. He received his PhD degree in Chemical and Biomolecular Engineering from North Carolina State University in Jan. 2022 under the supervision of Prof. Orlin D. Velev and Prof. Michael D. Dickey. His PhD research focused on developing wearable sweat based epidermal patches for lactate sensing that functioned on novel fluid withdrawing techniques.

Sneha Mukherjee

Sneha Mukherjee is currently a graduate student working with Prof. Orlin D. Velev and Prof. Michael Dickey in the Department of Chemical and Biomolecular Engineering at NC State. She joined in 2019 after completing her Masters from Indian Institute of Technology, Kharagpur (IIT-KGP). Her PhD thesis focuses on developing lateral flow assay (LFA) platform for sensing multiple analytes (cortisol, potassium) in sweat using non-invasive, zero-power techniques. She also works with DNA based nanoparticles.

of biomarkers (which are commonly found in blood and transferred from there to sweat and ISF), often without the need to visit a doctor.

The use of microfluidic platforms to manipulate biofluids enables rapid sample processing, operation with low reagent volume, control of molecules in space and time, and automation to avoid human intervention and error.[1,2] Various microfluidics technologies have been widely applied towards the development of biosensing platforms since the early 2000's[1–5] with human biofluid targets including sweat,[6] ISF,[7] saliva,[8] tears,[9] urine,[10] and blood.[11] Microfluidic platforms have been deployed for sensing either *via* wearable patches (on-body, which many reports refer to as '*in vivo*', inclusive of devices that rest on the skin) or through benchtop analysis (*in vitro* and *ex vivo*).

We focus here on sweat and ISF because of some of the challenges associated with other biofluids. For example, saliva is widely available in the mouth and continuous biomarker monitoring can be conducted by attaching wearable sensors directly on the inner mouth wall or on teeth.[12] Sensors can also be embedded in baby pacifiers for sampling and sensing.[13] However, saliva sensors always remain vulnerable to biofouling from the bacterial contamination arising from food or the mouth itself. Continuous monitoring with tears is possible using contact lenses with printed sensors. Tears can also be sampled *in situ* from the lacrimal caruncle and measured separately with a benchtop assay. On a similar note, sensors can be either embedded directly on diapers[14] for wearable urine monitoring or the urine can be sampled first and then monitored on the bench. Despite containing rich biomarker information, wearable platforms for such biofluids target only sensitive locations of the body, which eventually restricts them from long-term continuous data collection. Furthermore, urine and tears cannot be continuously generated for long-term (hours, days), while blood can be accessed only intermittently with fingerpicking. In contrast, sweat and ISF are easily accessed biofluids since sweat glands are abundantly distributed throughout the body[15,16] and ISF lies in close proximity to the blood capillaries.[17] Furthermore, both sweat and ISF include several key biomarkers that are present in blood. Examples include Na^+, K^+, Cl^-, lactate, alcohol, glucose, uric acid, cortisol, and proteins. Sweat gets released commonly whenever the body either undergoes active physical exertion due to elevation of the internal body temperature,[18] while ISF is usually accessed through skin-mounted devices that use techniques like reverse iontophoresis (RI)[19] or with minimally invasive tools like microneedles that can penetrate the top layer of the skin.[12] Hence, conducting on-body, continuous, and long-term sensing and analysis of sweat and ISF using wearable patches holds tremendous potential towards non-invasive health monitoring.

Several comprehensive reviews cover important aspects of sweat and ISF wearable sensors.[20–22] This review is distinguished by its focus on the microfluidic principles of sampling, sensing, and managing sweat and ISF collected using wearable patches. Given the emphasis on microfluidics, we point the reader to other reviews that focus on sensing.[16,22] We take a pedagogical approach with the hope this review will serve as a resource for new researchers as well as those actively working to improve devices in the future. The review is organized by following the physical path of sweat/ISF from the skin through the device: that is, it must first leave the skin, be collected by the device, transported through the device to sensing regions, and in some cases, evaporate as the fluid leaves the device. We begin by discussing the microfluidic aspects inside skin that govern the production of sweat and ISF, followed by their extraction techniques. Next, we focus on the microfluidic techniques executed in wearable prototypes to

Michael Dickey

Prof. Michael Dickey is a Camille and Henry Dreyfus Professor and University Faculty Scholar at NC State University. He received his Ph.D degree from University of Texas at Austin in 2006 and his postdoctoral training from Harvard University under Prof. George Whitesides. His group is studying new ways to pattern, actuate, and control soft materials (gels, polymers, liquid metals). Applications of his research includes patterning, 3D printing, stretchable/soft electronics, self-folding, actuation of soft robotics, wearable electronics, energy harvesting devices, reconfigurable circuits, and microfluidics.

Orlin Velev

Prof. Orlin Velev is a Frank and Doris Culberson Distinguished Professor at NC State University. He received Ph.D. degree from the University of Sofia, Bulgaria in 1996 and his postdoctoral training at the Department of Chemical Engineering at University of Delaware. He joined the Department of Chemical and Biomolecular Engineering at NC State in 2001. Prof. Velev has established a record of innovative research in the assembly of colloidal nanostructures with magnetic, electrical and photonic functionality, biosensors, microfluidics and nanomanufacturing. He has contributed more than 240 publications and more than 300 invited presentations. He has received numerous awards and has been elected as an ACS and MRS Fellow.

control the flow and sustain long-term device operation. Finally, we present the design strategies for an ideal sweat/ISF prototype based on varying physiological conditions and highlight the future directions and prospects of these microfluidic technologies.

2. The production and transport mechanisms of sweat and ISF

2.1 Sweat and ISF production mechanism

There are three main types of sweat glands present inside the human skin: eccrine, apocrine, and apoeccrine.[18] The density of eccrine sweat glands is the highest (~250–550 glands per cm^2) and they are the most common type of sweat glands in the entire body (~2–4 million in the entire body), with the highest density in palms and soles.[23] The eccrine glands consist of three sections: secretory coil, dermal duct, and upper coiled duct.[23] The secretory coil contains three types of cells: clear, dark, and myoepithelial.[18] The clear cells are mainly responsible for the production of sweat. The dark cells act as a repository for bioactive materials in sweat, while the myoepithelial cells provide structural integrity to the duct. The sweat production process is typically stimulated by heat, which initially causes an influx of Ca^{2+} into the clear cells. This results in an osmotic gradient in the clear cells, which causes water (sweat) movement into the lumen. In the luminal cells, ions and salts are continuously reabsorbed back through active and passive diffusion transport processes. The reabsorption rate relates inversely to the flow speed of sweat through the duct. Hence, lower absorption rates indicate higher electrolyte levels in the lumen. Capillary forces pump the sweat from the luminal cells along the length of the duct towards the skin, where it appears on the surface through the skin pores. Eccrine sweat is mainly composed of water, NaCl, and substances from the ISF.

ISF is the fluid between cells and is present at both the epidermal and dermal layers of the skin, with the dermis having the highest amount.[17] The blood capillaries lie in close proximity to the dermis and serve as the major contributor to the ISF constituents. Conversely, the lymphatic capillaries drain out fluid from the dermis, thus guiding the ISF transport from blood to lymphatic capillaries *via* dermis. Hence, the net amount of dermal ISF available for extraction depends on the lymphatic clearance rate, where both advective and diffusive forces govern the net ISF solute content.

2.2 Sweat and ISF transport mechanism from within the skin

The design of microfluidic wearables interfacing with skin can be aided by the understanding that the sweat is released by a natural microfluidic network in the skin. A detailed microfluidic model of sweat transport through the skin has been reported.[23] Briefly, sweat is driven out of the capillaries due to the osmotic pressure difference with respect to the sweat glands. The osmotic pressure of sweat in the sweat glands (ΔP_{osm}) is calculated using $\Delta P_{osm} = iRT\Delta C$, where i, R, T, ΔC represent van't Hoff factor (i = 1 for sweat), gas constant, temperature, and concentration difference between plasma and sweat, respectively. Assuming a surface tension of 72 mN m^{-1}, the maximum (ΔP_{osm}) engendered by the eccrine glands can be at least ~70 kN m^{-2} (~27 mOsm kg^{-1}), which is sufficient to overcome surface tension and thereby push the sweat into the duct (Fig. 1A). This estimated pressure is even high enough to push sweat even through a superhydrophobic (θ = 180°) pore of 2 μm diameter. The model assumes the pressure drop (ΔP) of sweat to be non-linear along the length of the duct, as it travels from the sweat glands to the external surface of the skin. The non-linear trends exist since sweat is continuously produced along the length of the duct and so the flow rate (Q) increases along the length of the dermal duct. Hence, the sweat glands can act as pumps to drive the sweat *via* pressure difference towards the skin surface. The pressure of the sweat droplet at the exterior surface of the skin can be evaluated by the Laplace pressure (P_L), $P_L = \frac{2\gamma \cos\theta}{a}$, where γ is the surface tension of sweat, θ is the contact angle of sweat on skin surface, and a is the radius of the droplet.[23] This equation is consistent with the following: (a) $P_L \to 0$ when $a \to \infty$ (due to spreading of sweat on the surface of the skin) or $P_L < 0$ when $90° < \theta \leq 180°$ (if sweat is wicked away). Overall, this whole transport mechanism is biomimetic to water transportation in plants – roots intake water by osmotic pressure differences with the soil and water transports *via* capillary action through the stem to the leaves.[24]

The ISF majorly lies in the dermal layer of the skin (~120 μL cm^{-2}).[17] Although this volume is high, the net amount of ISF available on the skin surface is usually low (~10 μL s) due to the high resistance offered by the skin layers during transport from capillaries to the interstitial space between the cells. Moreover, ISF has a slow replenishing rate from blood. Hence, unlike sweat, conducting long-term and continuous sensing with extracted ISF on skin is relatively difficult.

Once sweat and ISF are available on the skin surface, they are ready to enter the inlet zone of the device (Fig. 1B and C). Its dimensions will vary based on the biofluid extraction rate, volume, and time. The hydrodynamic resistance (depending on channel dimension, and material) of the channel will then decide whether the sweat/ISF can be transported. Usually, the channel can be made up of either polymer, fiber, or paper, and inherent hydrophilic materials like paper or fiber would be suitable candidates to transport low sweat and ISF volumes. Next, the fluid flow can be controlled and guided using valves. Usually, they are useful with high sweat volumes since it is easy to manipulate it in the channel. Finally, an outlet site is needed to dispose of the old biofluid and prevent its mixing with the newly extracted biofluid at the inlet. Usually, this is achieved with evaporation. Overall, the concurrent functioning of all these components will guide the efficient functioning of such wearable microfluidic prototypes.

2.3 Biomarker information in sweat and ISF

Sweat contains a wide variety of biomarkers that can be sensed.[25] These biomarkers can range from ions, metabolites, acids, hormones, and small proteins.[16,23] The

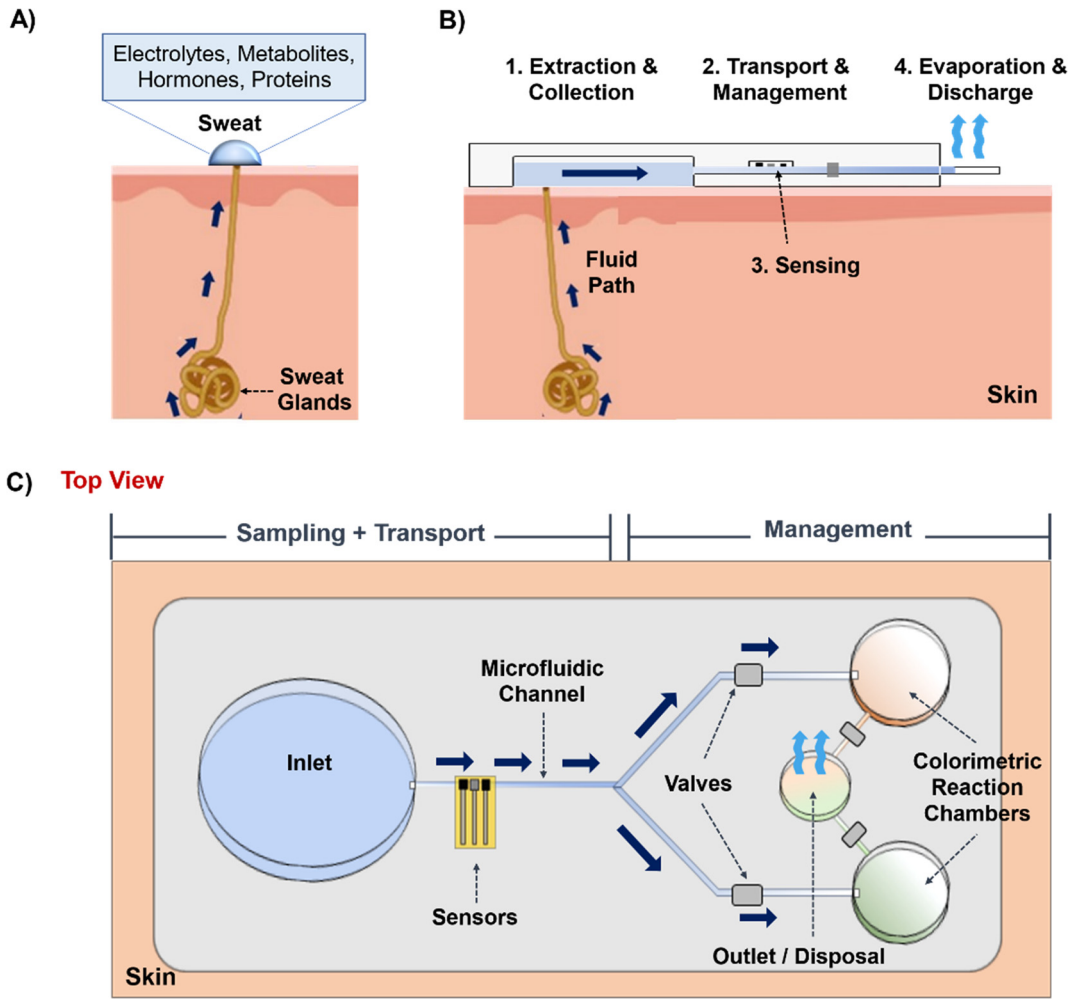

Fig. 1 An overview of the microfluidic aspects of wearable sweat and ISF sensing patches. (A) Sweat and ISF containing useful biomarkers can be extracted on skin non- or minimally invasively. (B) The extracted biofluid can then be transported through microfluidic channels to a desired analyzing location. Valves control the fluid flow, sensors interfaced with the channel can detect biomarkers, and evaporation facilitates prolonged sampling for longer durations. (C) Schematic with the top view of a microfluidic platform comprising all the essential components to withdraw, transport, and manage sweat and ISF.

transport mechanism of all biomarkers depends on several other factors such as their size, charge, and the physiological condition of the subject. Na^+ and Cl^- are the most abundant ion species in sweat, which are actively transported between blood and secretory coil due to the osmolality differences between the two. Ca^{2+} and K^+ concentrations are present in mM range. NH_4^+ diffuses into the sweat glands and stays ionized due to high sweat pH, which traps it inside the secretory coil and produces a concentration in mM range. Metabolic activity produces lactate and urea in sweat. The glucose presence in sweat is low (~μM range) since majority of blood glucose partitions to ISF. Proteins such as hormones and neuropeptides are also found in nM or pM traces since they are mostly filtered during their transport from the sweat glands to skin.[26] Alcohol, drugs, and heavy metals are also secreted in sweat.

The capillary pressure of the blood capillaries, the molecular weight, and surface characteristics of a biomarker are the major deciding factors for its availability in the ISF. Since most of the capillaries are leaky, nearly every biomarker in blood can potentially be found in ISF.[17] Paracellular and transcellular are the two dominant pathways governing biomarker migration from blood to the ISF. In paracellular transport, the biomarkers pass directly from blood to ISF through the cellular junctions of the blood capillaries, while in transcellular transport, the biomarkers move from blood to ISF through the cell itself.[27] Small hydrophilic (ions, glucose, urea, lactate) and hydrophobic (cortisol) molecules (<3 kDa) usually undergo paracellular transport. Medium-sized molecules (3–70 kDa) such as insulin, hemoglobin, and cytokines undergo both paracellular and transcellular transport since the tight cellular junctions impede pure paracellular transport. Molecules above 70 kDa (albumin, immunoglobulins) only undergo transcellular transport as they cannot pass through the intercellular junctions.

3. Sweat and ISF withdrawing techniques from skin

3.1 Sweat withdrawing techniques

Sweat can be generated on the skin surface using the following general techniques: (a) active perspiration, (b) thermal stimulation, (c) chemical and electrical stimulation, (d) osmosis, and (e) diffusion. Undergoing strenuous physical exertion (active sweating) is the most common way to generate sweat. The rate of sweat generation through active perspiration is high (1–3 μL min^{-1}).[28] Fig. 2A shows an example of a subject undergoing physical exertion to release sweat into microfluidic wearable platform (yellow dotted circle) on the forearm for conducting multi-biomarker sensing.[28] The reported platform in the paper uses a serpentine polydimethylsiloxane (PDMS) microfluidic system to collect sweat and transfer it to printed electrodes for simultaneous sensing of sweat rate, ionic charge, and Na^+ levels. Several PDMS microfluidic platforms have been developed on similar principles to monitor various biomarkers in sweat during active perspiration.[29–32]

Another common way of naturally generating considerable amount of sweat on the skin surface is *via* thermal

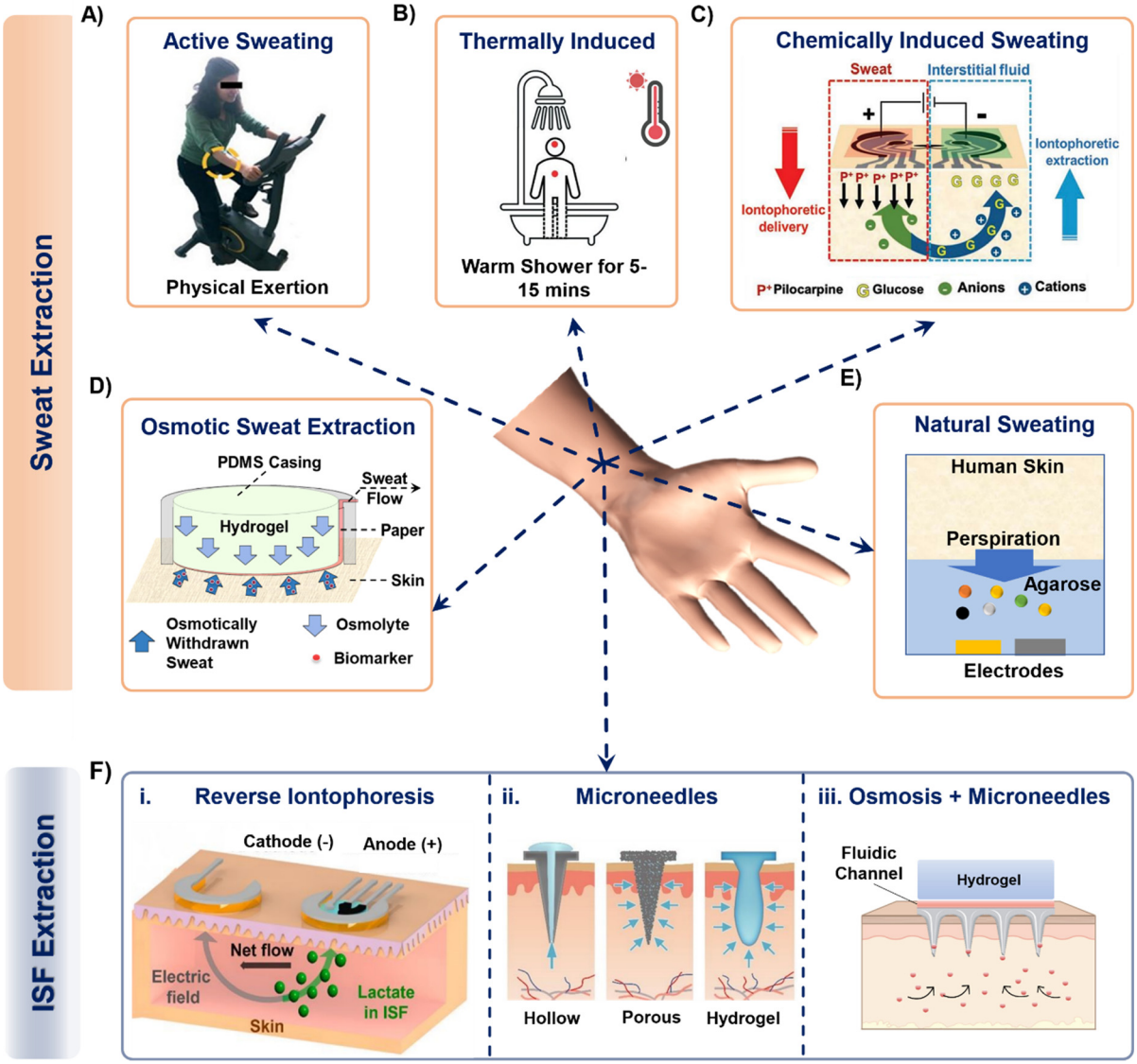

Fig. 2 Examples of techniques that collect sweat from the body into a sensing device. Sweat from the skin surface can be generated by either making the subjects undergo (A) strenuous physical exertion or (B) thermally induced exertion. Adapted from ref. 28 and 33 with permission from Royal Society of Chemistry. (C) Invasive procedures such as passing small magnitude of current through skin surface can also generate sweat. Reproduced from ref. 38 with permission from John Wiley and Sons. (D) Hydrogels with higher osmotic strength than sweat can withdraw sweat directly from the skin surface while the subject is at rest. Adapted from ref. 43 with permission from American Chemical Society. (E) A hydrogel (with high water content) can sample sweat biomarkers directly from skin surface, such as from fingertips. Reproduced from ref. 48 with permission from Springer Nature. (F) Interstitial fluid extraction methods using (i) reverse iontophoresis, (ii) hollow, porous, and hydrogel-based microneedles and (iii) osmosis enabled microneedles. Reproduced from ref. 19 and 49 with permission from Elsevier.

stimulation. This is done by exposing the subjects to high temperature conditions such as a hot shower or sauna.[33–35] Such conditions increase the rate of sweating (Fig. 2B). Sweat stimulated thermally (hot shower) has been sampled in PDMS microfluidic wearable patches, which collect up to 4–5 μL of sweat within 15 minutes to measure creatinine, urea, and sweat pH.[33] A similar PDMS microfluidic patch measured Na^+, K^+, and lactate in sweat from the chest, forearm, and back of the body by exposing the subjects to dry sauna for 30–40 minutes.[34] In a recent study, a poly(methylmethacrylate) (PMMA) microfluidic patch was developed to monitor sweat nutrients (vitamin C, calcium, zinc, and iron) by exposing the subjects to a sauna for 50 min during which time ~30 μL of sweat was sampled.[35] Although sweat generation *via* thermal stimulation does not involve exhaustive physical exercise and leads to reasonable sweat rates, continued exposure for long time periods inside a high temperature environment can be inconvenient, uncomfortable, and detrimental to the skin.[36] Moreover, measuring biomarkers from actively generated sweat can raise questions regarding rapid saturation of the channel, and dilution from excessive sweating.

Given the above limitations, several reports present other alternative sweat withdrawing techniques that involve lesser exertion than active sweating and thermal stimulation. One such technique involves inducing sweat production chemically through transdermal delivery of drugs like pilocarpine and carbachol.[37–39] These drugs are cationic in nature and are infused and delivered into the skin surface *via* iontophoresis (IP). IP is an established process to induce ions or charged molecules to flow into the skin by applying current (0.2–0.5 mA cm^{-2}) through the skin surface. The drugs are loaded in a hydrogel on the anode and delivered across the skin by applying an electric field (Fig. 2C). As a result, all of the anionic species in sweat move towards the anode due to their electrophoretic mobility, while all the cations and neutral species (like glucose as shown in Fig. 2C) move towards the cathode due to electrostatic attraction and electroosmotic flow. The volume of extracted sweat can range from 15–100 μL, depending on the applied current density and operating time.[40] Although iontophoresis can operate under sedentary conditions for prolonged periods (>24 hours),[41] the possibility of skin irritation always remains a potential issue due to the involvement of electric current. Moreover, material defects (such as low hydrogel thickness, and drug overdose) in the system can also affect the sampling rate.[42]

Our group has introduced an osmotic collection technique that can withdraw sweat from subjects at rest by simultaneously using osmosis for sweat withdrawal, capillary forces for sweat transport, and evaporation for long-term sweat management (Fig. 2D).[43–47] The prototype shown in Fig. 2D has two major components: hydrogel and paper microfluidic channel. The withdrawal of sweat from the skin is achieved using a hydrogel, which has a higher solute concentration than sweat. Once the hydrogel contacts the skin, the chemical potential difference between the gel and skin makes the sweat and its associated biomarkers move from the skin towards the hydrogel. The sampled sweat can be transported either by using a conventional microfluidic channel[47] or a paper strip conduit.[43] The sweat flow can be sustained for ~10 hours through continuous evaporation of sweat at the back end of the paper channel.[44] Notably, osmosis does not depend on any other external factors (physical exertion levels, surrounding temperature, and current density) since it is a colligative property. Hence, osmosis has the potential to be a completely painless, and non-invasive sweat sampling technique under low sweating conditions. However, this technique leads to collection of low sweat volume (2–5 μL with polyacrylamide hydrogels in 2 hours) for individuals at rest. Special attention is also needed for the overall patch design to prevent sweat evaporation.

Researchers have also used hydrogels to withdraw sweat from the skin *via* diffusion.[48,50–54] The first platform designed to demonstrate this technique is shown in Fig. 2E.[48] The platform was developed using thin agarose hydrogels which were directly interfaced onto the functionalized electrodes for sweat lactate sensing. The hydrogel acts as a reservoir for sweat biomarkers and an electrolyte to allow electrochemical detection. Sweat lactate was collected *via* touching the gel with the fingertip for ~200 seconds since the human fingertip has high sweat gland density.[55,56] As a result, the lactate generated from the fingertip due to the natural sweating diffuses through the hydrogel to reach the electrodes, where it undergoes an enzymatic reaction to generate a signal change. Although such a platform provides painless biomarker detection at rest, these devices are not in wearable format, do not contain an enclosure to seal the hydrogel to prevent it from drying (useful for long-term operation), and do not provide information regarding the collected sweat volume.[48,50–52,54] Hence, the continuous and long-term (~hours) performance of these platforms remains a challenge.

3.2 ISF withdrawing techniques

The ISF can be extracted using techniques such as capillary wicking, vacuum suction, micro dialysis, reverse iontophoresis (RI), and with tools such as microneedles.[17] Amongst these, RI and microneedles are predominantly used due to their minimal invasive impact on skin and their capabilities to generate stable and continuous biomarker profiles. RI operating mechanism is similar to IP but without the initial drug delivery. Fig. 2F(i) shows the mechanism of a typical RI setup on the skin for ISF lactate extraction.[19] Usually, applying a current density of 0.4 mA cm^{-2} on skin for 10 min is sufficient to extract ISF. RI faces the following limitations: (a) the electrical current can cause skin irritation. (b) It cannot be sustained long-term (c) the volume of extracted ISF is very low (~nL). (d) The presence of hydrogel in between the electrode and skin causes analyte dilution and makes it difficult to extract biomarkers whose concentration in ISF is low (such as proteins, and hormones).

Another way of accessing and extracting ISF is by using microneedles.[63,64] Microneedles penetrate the dermis layer of the skin, but are short enough (<700 μm) to avoid contacting nerves and are therefore considered to be minimally invasive. They can be solid, soft, and hollow. Solid microneedles can be made of metal, silicone, and resins and are fabricated using either 3-D printing, etching, or laser cutting. The sensing components can be functionalized on the tip of the needle, allowing them to directly interface with the ISF inside the skin.[65] Alternatively, ISF can be extracted with solid hollow microneedles using vacuum and capillary action, which can lead to ~15 μL's of ISF in rats.[66] Soft microneedles are usually made up of hydrogels and can be either solid or porous. They collect ISF *via* swelling (Fig. 2F(ii)).[49] Despite their potential, such microneedles are reported to extract more ISF volume in rats, mice, and pig models than from human skin.[63] Moreover, microneedle insertion can even elevate the levels of inflammatory markers in the body, eventually increasing the chances of registering false positive signals when targeting to measure such biomarkers.[67] Our group has recently demonstrated how osmosis can be utilized to prolong ISF collection (US patent #18/217392). Interfacing a high osmotic strength hydrogel and a paper channel to the back of a soft microneedle patch enables prolonged ISF sampling and flow for continuous biomarker monitoring (Fig. 2F(iii)).

To summarize, this section focuses on the ways in which sweat and ISF can be generated or extracted from the skin. Sweat extraction approaches *via* exercise, thermal, and chemical stimulation could be stressful/inconvenient and may not be feasible for long-term (hours to days) operations. However, they result in considerable sweat volume generation and quicker appearance of sweat on the skin surface. We summarize the operational parameters of devices based on different principles in Table 1. Sweat collection *via* osmosis and diffusion using hydrogels offer a pain-free, non-invasive alternative under low sweating conditions (such as at rest or low humidity surroundings) but results in lower sweat volume generation over time and requires more time for the sweat to reach the skin surface. There are no reports available about the estimated sweat rates for the prototypes solely relying on diffusion for biomarker sensing. ISF can be sampled using RI and microneedles, where RI applies electric field on skin to facilitate rapid biomarker appearance on skin with negligible fluid volume. Microneedles require an external pumping source to withdraw the sampled ISF and are more widely used for ISF sensing and extraction. Hence, all withdrawing techniques possess certain advantages and disadvantages.

Once the sweat and ISF are accessed, the next challenge is to transport, manage, and sense the biomarkers in sweat and ISF. Hence, the next section is focused on the design aspects of various microfluidic patches for transport and management of sweat and ISF.

4. Fluid transport using microfluidic techniques

Once the sweat is extracted to the skin surface, various microfluidic tools can be used for its collection and transportation. Processing of sweat using microfluidic channels is necessary since direct interfacing of the sensor with sweat on skin can raise questions regarding its clean capture, external contamination, and measurement errors from uncontrolled evaporation. The fundamental governing equations for pressure-driven fluid flow inside microfluidic channels assume Poiseuille relations (Fig. 3A(i)): $\Delta P = \frac{128\mu LQ}{\pi d^4}$ (for circular channels) and $\Delta P = \frac{12\left[1-\frac{192H}{\pi^5 W}\tanh\left(\frac{\pi W}{2H}\right)\right]^{-1}\mu QL}{WH^3}$ (for rectangular channels)[68] where ΔP is the pressure drop between the inlet and outlet of channel and μ is the liquid viscosity (typically 0.001 Pa s for sweat). Q, d, L, W, H represent the volumetric liquid flow rate, diameter, length, width, and height of the channel, respectively. The above equations show how fluid flow rates in microfluidic channels depend on the channel dimensions; in particular, the flow rate is especially sensitive to the cross-sectional geometry (*e.g.*, note the d^4 and L, W, H dependency). The pressure (ΔP) required to transport liquids can arise from capillary forces (requiring favorable wetting), evaporation, or osmotic gradients between the inlet and outlet. More details on how ΔP correlates to the channel diameter are discussed in detail in the latter half of section 4.

Table 1 Sweat and ISF extraction techniques and their reported operating parameters

Extraction technique	On-body location	Device sampling area (cm^2)	Generated rate ($\mu L\ min^{-1}\ cm^{-2}$)	Time to reach skin surface (min)	Ref.
Active sweat	Forearm, forehead, back, upper arm, back, thighs	3–7	1–5	5–15	6, 57–59
Thermal stimulation of sweat	Forehead, chest, back, arm	1–4	3–9	<10	33, 35
Chemical stimulation of sweat	Forearm, upper arm	1–2	1.5–3	5–10	37, 38, 60
Osmosis of sweat	Forearm	0.2–0.5	0.07–0.3	30–45	43, 44, 61
Diffusion of sweat	Fingertip	2–3	N/A	<30	50–52
Electrical stimulation of ISF	Forearm	0.2–0.4	N/A	5–10	19, 62
Microneedles for ISF	Forearm	0.25–0.5	1–3 in pigs, mice, rats N/A – humans	3–10 min – rats, mice, pigs Humans – N/A	63

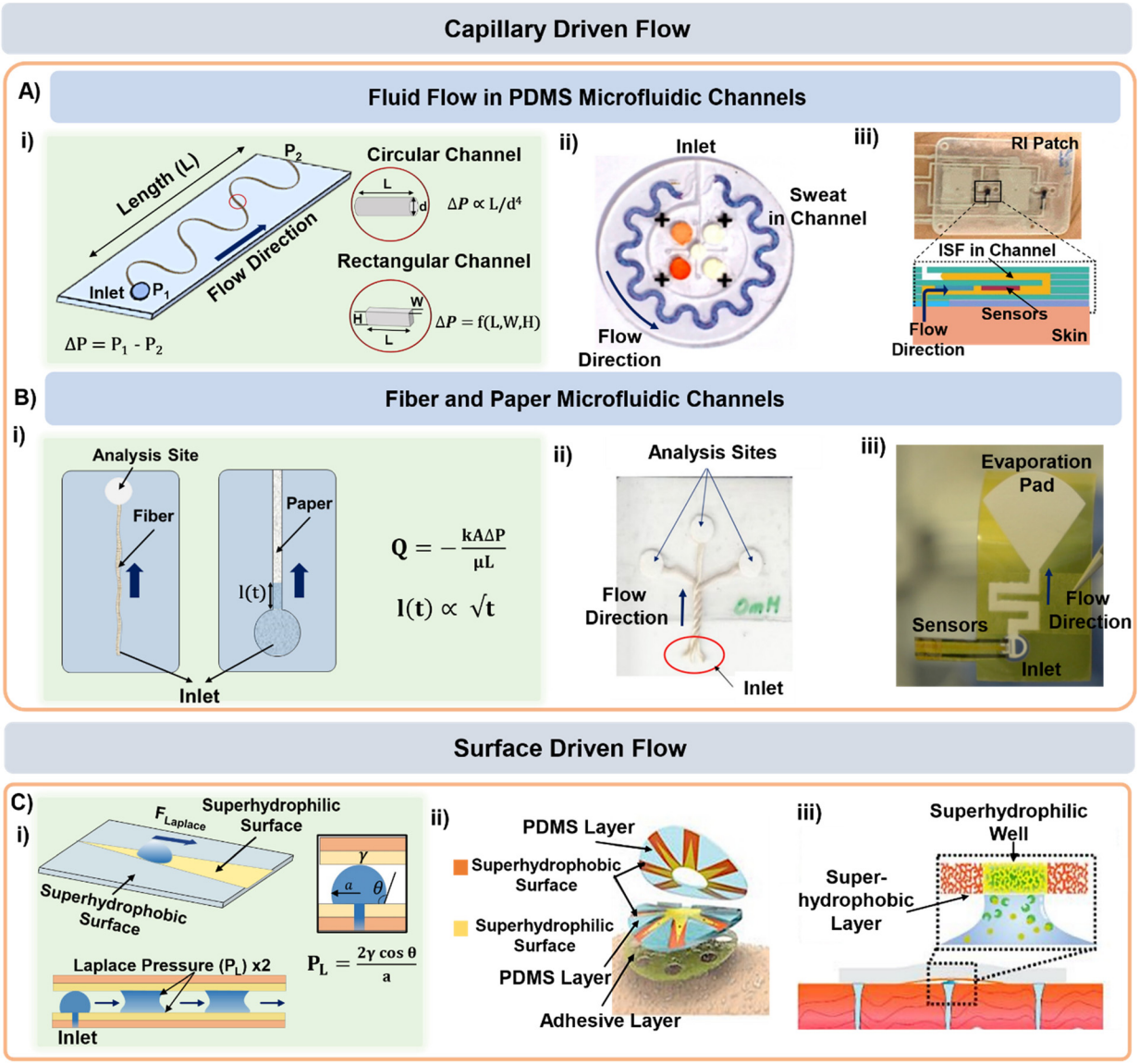

Fig. 3 Sweat and ISF transport in microfluidic channels. A) (i) Schematic highlighting the dimensional aspects of a typical microfluidic channel. PDMS and PET microfluidic channel-based lab-on-a-chip form factors for (ii) sweat and (iii) ISF transport. Adapted from ref. 6 and 7 with permission from American Association for the Advancement of Science and Royal Society of Chemistry respectively. (B) (i) Schemtic highlighting the parameters governing fluid transport in fiber and paper microfluidic based devices. Examples of (ii) fiber and (iii) paper microfluidic based devices for sweat transport. Adapted from ref. 73 and 61 with permission from John Wiley & Sons and American Chemical Society respectively. (C) (i) Surface morphology based sweat transport driven by superhydrophilic and superhydrophobic patterned layers in (ii) wedge-shaped channels and (iii) microwells. Adapted from ref. 74 and 30 with permission from John Wiley & Sons, and American Chemical Society respectively.

Conventional (PDMS based) microfluidic channels have been used routinely for sweat transport in wearable devices (Fig. 3A(ii))[6,37] where the sweat is collected *via* both active perspiration and IP. Since PDMS is hydrophobic, it is usually treated with oxygen plasma to make the surface hydrophilic prior to usage and thereby create favorable wicking conditions (*i.e.*, ΔP arising from capillary forces). PDMS is commonly used for sensing and transporting hydrophilic molecules.[69] Such devices have been widely established for sensing glucose, lactate, chloride, and pH in sweat. Macroduct® sweat collector is a commercial microfluidic platform that has been routinely used during on-body trials.[70] It consists of a spiral tube (inner diameter 640 μm) with an orifice that opens directly to the skin. The maximum volumetric capacity of these patches is ~85 μL and they are mainly used for sweat rate measurements.[71] The tube comes filled with a dye. The position of the dye front upon sweat intake gives an estimate of the sweat volume and release rate. Macroduct® patches are designed to minimize the dead space between the device and skin to maximize sweat collection.

Microfluidic transport has also been utilized for ISF transport in wearable form factors.[7,72] The wearable prototype shown in Fig. 3A(iii) utilized RI to sample ISF in a

PET microfluidic channel. The ISF flow rate was measured to be 0.9 μL min^{-1} and chloride and calcium ions were measured electrochemically for up to 15 min. Microneedle-based ISF sampling and microfluidics have also been utilized to measure metabolite (glucose and lactate) levels.[72]

Microfluidic devices based on fabric and paper have also been used for sweat sampling and transport due to their wide availability, inherent hydrophilic nature, and usage convenience without any complex fabrication steps (Fig. 3B(i)).[73,75–78] The wicking flow in such devices is analogous to capillary flow in porous media, which is governed by the original Lucas–Washburn equation: $l(t) = \sqrt{\frac{\gamma r t \cos\theta}{2\mu}}$ (without evaporation) and its modified version: $l(t) = \sqrt{\frac{\gamma r \varnothing h t \cos\theta}{4\mu q_o}\left(1 - e^{\frac{-2q_o t}{\varnothing h}}\right)}$ (with evaporation),[79] where $l(t)$, γ, r, θ, t, μ, h, q_o, $\varnothing$ represent the distance travelled by sweat in paper over time, sweat surface tension (~70 mN m^{-1}),[23] average pore radius of paper (~5–10 μm), sweat contact angle, time, sweat viscosity (0.001 Pa s), thickness of the paper, evaporation rate, and porosity of paper respectively. These equations are derived assuming constant cross-section, chemical homogeneity, unlimited reservoir volume, and negligible gravity effects. These equations show that: (a) the length of water penetration in the paper channel levels off over time due to viscous drag and (b) evaporation can decrease the length of water penetration. Alternatively, Darcy's law is also used to describe fluid flow through porous media and is applicable to substrates with non-uniform pore sizes.[80] Darcy's law assumes that the kinetic energy of the fluid flow is negligible, the fiber cross-section is circular, and the capillary is straight. It can be expressed through the equation: $Q = -\frac{kA\Delta P}{\mu L}$, where Q is the volumetric flow rate, μ is the fluid viscosity, k is the permeability of the paper, L is the length of the paper, A is the cross-sectional area of the paper perpendicular to the fluid flow direction, and ΔP is the pressure difference acting across the paper.

As an example, both cotton fabric and non-woven fabrics can be used to transport sweat.[75,76] In another example, a fiber thread has been used to transport sweat to the sensing zone on paper (Fig. 3B(ii)).[73] However, this was only shown as a proof-of-concept for *in vitro* glucose sensing. Sweat sampling and sensing have also been conducted using only paper microfluidic channels. The sensor can be either directly attached[77] or interfaced to the paper orthogonally.[46,61,78] Our group has also developed a versatile paper microfluidic platform for sweat lactate sensing from both passive and active perspired sweat (Fig. 3B(iii)).[45,46] The prototype can generate real-time sweat lactate profiles under any physiological condition. Similar devices also exist for measuring lactate, pH, and sodium levels in sweat under active perspiration.[77,78]

The surface morphology of a microfluidic channel can also be modified to guide the sweat and ISF flow. For example, a patch with "cactus spine" inspired hierarchical micro-structured channels can sample and transport sweat (Fig. 3C(i and ii)). The patch consisted of wedge-shaped (similar to cactus spine shape) PDMS microfluidic channels whose surface was modified with both superhydrophilic and superhydrophobic coatings. The coexistence of both coatings generated a asymmetrical wettability gradient and the wedge shape supported fast transport by generating a force (from Laplace pressure) along the direction of the superhydrophilic area. Sweat flowing through the channel got collected into a microwell containing an enzymatic electrochemical sensor for lactate and glucose sensing.[74] Based on a similar concept, microwells with hydrophilic (wettable) walls have also been used as components of sweat sampling devices (Fig. 3C(iii)).[30] For example, a superwettable flexible band with superhydrophilic microwells surrounded by superhydrophobic edges can collect sweat and host colorimetric assays. The superhydrophobic sections ensured that fluid collection only occurred through the superhydrophilic zones.

Overall, microfluidic platforms for sweat and ISF transport have been extensively investigated, using either conventional PDMS/PMMA/PET microfluidic channels or thread/paper wicking materials. Both colorimetric and enzymatic assays can be integrated with such devices. However, since considerable sweat rate (20–200 μL h^{-1} cm^2) is required prior to sensing, these microfluidic platforms have been validated mostly on-body with active perspiration. Moreover, only a few wearable microfluidic prototypes have attempted on-body ISF sampling.[7,81] The net ISF sampled volume depends on the microneedle material, size, density, and exposure time. Solid microneedles will extract more with higher vacuum pull and lower capillary diameter, while porous, soft microneedles will hold more ISF than their solid counterparts.[82] Sweat and ISF transport and management are needed next for prolonged sensing and sampling. Hence, the next section highlights ways of sweat management in microfluidic channels.

5. Fluid management techniques in microfluidic channels

Once the sweat or ISF is collected in the microfluidic device, it is important to manage it efficiently for analyzing biomarkers, reducing contamination, achieving prolonged sensing, and delaying saturation due to complete filling of the channel. In the simplest case, fluid can just flow through a channel past an embedded sensor or to a reservoir for colorimetric sensing.

There are circumstances in which the fluid flow requires better control. For example, the flow can be directed by capillary burst valves (CBVs) as exemplified in Fig. 4A.[34] CBVs are commonly used to control flow and connect microchannels of either different diameters or surface properties (as shown in the left schematic in Fig. 4A).[83,84] The incoming liquid stops at the valve until the driving pressure overcomes the resisting capillary pressure. Once the driving pressure reaches a critical point, the fluid pushes beyond the valve, and the remaining channel gets wetted by the advancing liquid.

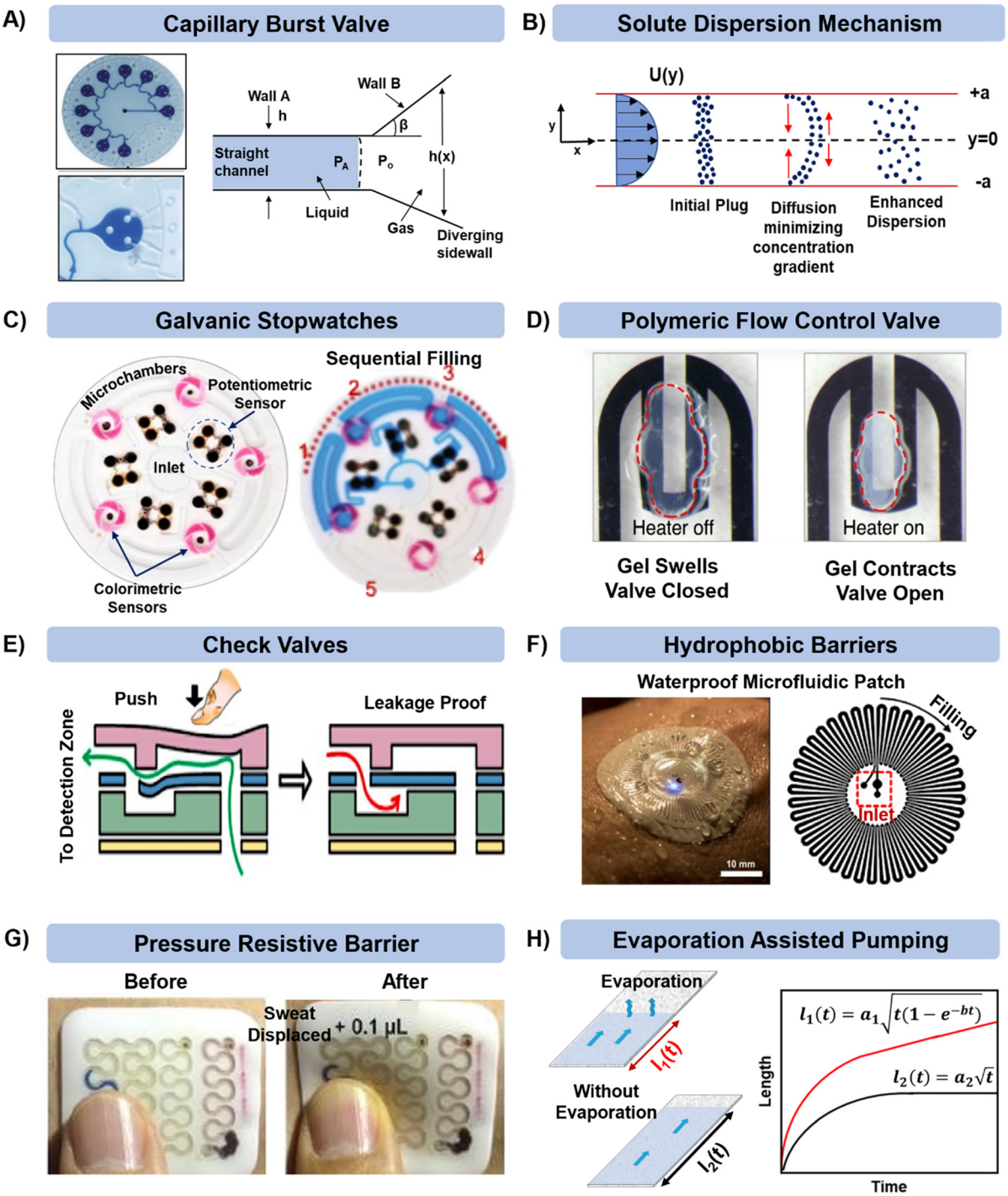

Fig. 4 Microfluidic technologies for managing sweat in microfluidic patches. Controlled and sequential analysis of sweat biomarkers in microfluidic channels can be achieved by (A) including capillary burst valves (adapted from ref. 34 with permission from John Wiley & Sons), (B) tracking solute dispersion time, (C) deploying potentiometric sensors (adapted from ref. 86 with permission from John Wiley & Sons), and (D and E) including polymeric and check valves (adapted from ref. 87 and 88 with permission from Springer Nature, and American Chemical Society respectively). External contamination, biofouling, and damage can be prevented *via* (F) material selection (adapted from ref. 89 with permission from American Association for the Advancement of Science) and (G) by providing reinforcement with polymeric layering (adapted from ref. 90 with permission from John Wiley & Sons). (H) Prolonged sweat collection can be achieved by having a pad for sweat evaporation in the patch. Analytes can collect and concentrate in this region for archival sensing (adapted from ref. 91 with permission from American Institute of Physics).

The microfluidic patch shown in Fig. 4A has 12 microwells in total. The wells are connected by microchannels and each well includes three CBVs. Each CBV in the patch of Fig. 4A has been designed to accommodate different bursting pressure (BPs) levels to allow sequential sweat flow to subsequent wells. The BP for a microfluidic

channel can be quantified using the equation: $\mathrm{BP} = (P_A - P_o) = -2\sigma\left[\frac{\cos\theta_1}{b} + \frac{\cos\theta_2}{h}\right]$, where, P_A and P_o are the pressure values of the liquid and gaseous phase, respectively, σ is the surface tension of liquid, θ_2 is the contact angle of the liquid in the channel, θ_1 is the minimum $[\theta_2 + \beta; 180°]$, β is the diverging angle of the channel, b and h are the width and height of the diverging section of the channel respectively (Fig. 4A).[83] From the BP equation it is seen that for a constant h, BP will be high under low b and $\beta > 90°$, while low under high b and $\beta < 90°$. A high BP would enhance the CBV to burst and spread the liquid throughout the channel.[83,85]

Along with flow control with valves, the time lag (t_{lag}) between the introduction of sweat in the channel and its arrival to the sensor, and the dispersion time ($t_{dispersion}$) of the liquid plug inside the channel are also important parameters that should be taken into consideration in microfluidic settings (Fig. 4B):[92] $t_{lag} = \frac{V}{Q}$ and $t_{dispersion} = \frac{2\sqrt{\left(D + \frac{d^2u^2}{192D}\right)t_{lag}}}{u_{avg}}$, where V is the channel volume, Q is the fluid flow rate, D is the molecular diffusion coefficient, and u_{avg} is the average fluid velocity in the channel. These effects can be further interpreted through the Taylor–Aris dispersion model for laminar flow (as shown in the right schematic of Fig. 4A). The schematic shows that once the sweat enters the channel, the solute molecules initially behave like a plug mimicking the shape of the flow. The shear forces induce lateral concentration gradients which molecular diffusion tends to minimize. Hence, the solutes experience an enhanced diffusive longitudinal spreading as sweat progresses downstream in the channel, which governs the t_{lag} and $t_{dispersion}$.

Another important consideration is determining the flow rate through the device (for further discussion, see section 7.1). Fig. 4C shows how potentiometric sensors embedded inside microfluidic channels can be used to record a timestamp of the biomarker flow and concentration.[86] As sweat passes through this sensor in the channel, the sensor starts discharging from its open circuit potential (OCP) and charges back again with analyte inflow. The final operating voltage and the time taken to reach it for each sensor gives an estimate of the sweat flow rate in the channel.

Gels can also be used in valves. For example, poly(*N*-isopropylacrylamide) (PNIPAM) is a hydrogel that swells significantly when the temperature gets below a critical temperature (Fig. 4D).[87] Thus, by using resistive heaters, it is possible to dictate when the valve opens. Heating the gel beyond the so-called lower critical solution temperature (LCST) allows sweat flow in the channel. The flow stops when the temperature gets below LCST. Check valves activated mechanically by a finger touch have also been used to control sweat flow inside microfluidic patches (Fig. 4E).[88,93]

Contamination of the microfluidic patches upon sweat collection can be prevented by judicious selection of the wall materials such that they remain inert to changes in the external environment. One such example is shown in the microfluidic sweat patch presented in Fig. 4F, which includes a layer of a hydrophobic polymer.[89] The layer has low water vapor permeability (both external and evaporation from inside the channel) and functions by maintaining robust adhesion with skin even during underwater swimming. On a similar note, the microfluidic patch shown in Fig. 4G included a rigid exoskeleton layer (made of commercial silicone) surrounding the microfluidic channel.[90] This made the patch resistive to external stresses (compression, impacts and acceleration) and prevented excessive fluid displacement in the channel.

Maintaining long-term sweat sampling is desirable, but in many devices the microfluidic capacity becomes saturated and sweat stops flowing into the device. This issue can be avoided by adding a section for sweat evaporation at the end of the microfluidic patch and increasing the surface area of paper.[61] Continuous evaporation maintains the capillary pressure in the channel by preventing the channel from complete wetting, which facilitates long-term inflow of sweat and consequently delays the device saturation. The modified Lucas Washburn equation accounting for the evaporative effects is mentioned in the explanation of Fig. 3B.[94] We have introduced such designs in paper microfluidic platforms for both *in vitro* (Fig. 4H)[91] and *in vivo* settings.[43,44,61] However, one should be careful with microfluidic designs involving evaporation since the paper pad will eventually be crusted by the salt deposits from the sweat, ultimately suppressing the evaporation rate. These concentrated deposits could be useful for archival sensing of components in sweat.

6. Design considerations for sweat and ISF microfluidic prototypes

Overall, an efficient sweat microfluidic sensing prototype should be designed by considering the factors summarized in Fig. 5A–D and Table 2:

a. The location for placing the patch on the body should be decided first by considering comfort and sweat gland density, followed by the type of biomarker to be sensed (see section 7). Any hydrophobic biomarker (*e.g.*, cortisol) would require additional surface modifications to prevent them from adhering to the walls of PDMS microchannels.

b. Next, the sweat extraction method should be decided – active or passive (Fig. 5A and B). For sweat to flow inside the channel, the secretory pressure of the sweat glands (P_{sec}) should exceed the hydraulic pressure loss (ΔP_{hyd}) in channel. This balance should dictate the overall channel design. High sweat volumes are obtained on-skin during active sweating due to high P_{sec} of the sweat glands. Also, higher sweat flow rates and smaller cross-sectional area of the channels build up pressure inside the channels. Typically, a patch placed on the forearm (150 glands per cm^2) with active perspiration (~10 nl min^{-1} per gland) can generate a sweat rate of 1–1.5 μL min^{-1} cm^{-2} on skin. Thus, a 1 cm^2 sampling area with 1 h operating time generates a total of 60–100 μL of sweat. Considering a channel of 1000 μm

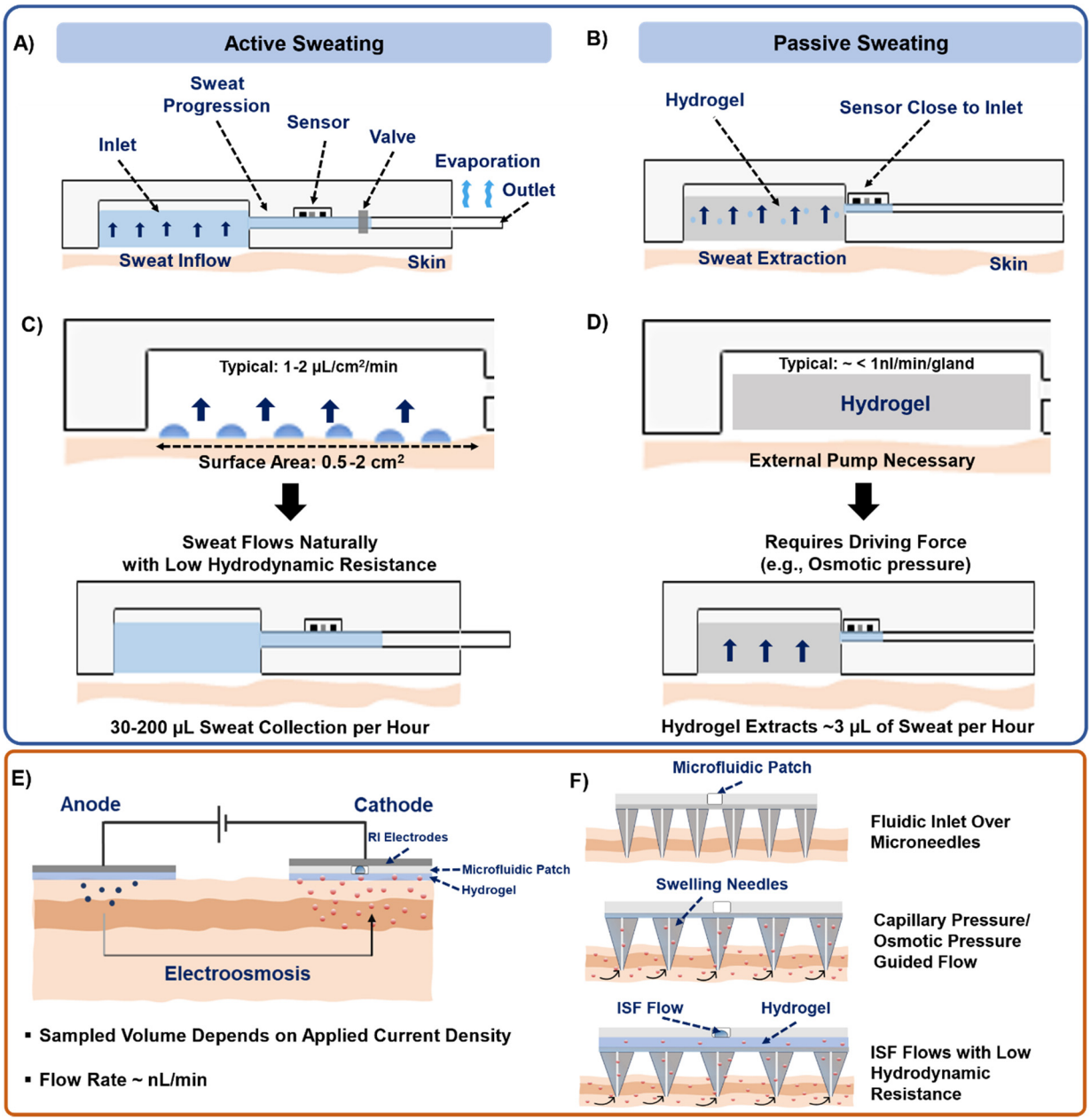

Fig. 5 Design strategies for microfluidic devices for sweat and ISF analysis. Schematics highlighting the position of different components of microfluidic devices functioning under (A) active perspiration and (B) passive perspiration. Schematic showing the necessary conditions required to push the sweat into the microfluidic channel with approximate fluid calculations under a hypothetical case of placing the device on the forearm during (C) active perspiration and (D) passive perspiration. (E) Schematic of microfluidic integration with a RI patch for ISF extraction. (F) Schematic highlighting the governing parameters for guiding ISF flow into a microfluidic channel with microneedles.

Table 2 Summary of the components of sweat microfluidic devices and their design specifications. See section 6b for the definition of the terms

Device consideration	Active sweat extraction	Passive sweat extraction
Inlet pressure	$P_{sec} > \Delta P_{hyd}$	$P_{osm} \gg P_{sec}$
Channel dimension	Width: 100–1000 µm, height: 50–300 µm, length: 1–10 cm	High channel cross-sectional area and lesser channel length preferred
Sensor location	Can be far from inlet	Close to inlet
Outlet	Large surface area (~cm^2)	Not necessary

width, 100 μm height, and 1 cm length, whose hydraulic resistance ($R_{channel}$)[53] can be calculated as: $R_{channel} = \frac{12\left[1 - \frac{192H}{\pi^5 W}\tanh\left(\frac{\pi W}{2H}\right)\right]^{-1}\mu L}{WH^3}$, would result in ~1.14 × 10^8 Pa s m^{-3} and corresponds to the hydraulic pressure drop of ~6.8 kPa, which is low in comparison to the sweat gland secretory pressure (~70 kPa)[23] under active sweating. Hence, sweat will be pushed into a microfluidic channel with such dimensions (Fig. 5A and C). The position of the sensor can be away from the inlet due to availability of sufficient sweat volume. Moreover, such conditions are also suitable for monitoring biomarkers (electrolytes, lactate) which depend heavily on the sweat rate. Saturation occurs when the microchannel fills with sweat. A sweat disposal mechanism (*e.g. via* evaporation)[91] can allow continuous inflow of fresh sweat to enable long-term monitoring. To date, most devices saturate after times ~hours, whereas 'long-term' refers to ~days/weeks; the time depends on the sweat rate, device volume, and disposal mechanism.

c. The passive sweat generation rate is very low (<1 nl min^{-1} per gland), and the secretory pressure of the glands is not significant to push the sweat into the channel. Thus, an external means of pumping (such as osmotic hydrogel) is needed for sweat withdrawal (Fig. 5B and D). The chemical potential of water in the hydrogel must be lower than in sweat (hydrogel has greater osmotic pressure P_{osm}). Based on the reported sweat rates under sedentary conditions from forearm (5–30 nL min^{-1} cm^{-2}),[44,53] only ~1–5 μL h^{-1} would be accessible on the skin. Hence, shorter channel lengths and a sensor located close to the sampling zone are needed. Alternatively, paper and thread-based microfluidics could be more effective in transporting media under such low flow rates since they are inherently hydrophilic by nature, or the sensing could be conducted at a high sweat gland density location (such as fingertip).[56] Such conditions could be useful for sensing biomarkers that have low concentration (*e.g.*, glucose, proteins, cytokines) in sweat. Sweat disposal mechanisms can be optional for both single-use and continuous devices.

The design of an efficient ISF sensing microfluidic prototype should be developed with the following considerations:

a. The ISF extraction can be performed using RI or microneedles (Table 3). The P_{sec} will depend on the applied current density and duration (Fig. 5E). Usually, 1–1.5 mA of current for a few minutes can only generate a few nL min^{-1} of ISF flow rate. Hence, the possibility of $P_{sec} < \Delta P_{hyd}$ will be high and ISF flow into the channel will be prevented. This is also the reason why there have been very few attempts to combine RI with microfluidics.

b. The sampling of ISF with microneedles will be guided by the capillary pressure (P_{cap}) of ISF (Fig. 5F). Usually, P_{cap} ranges ~0.25 kPa in a channel of 1000 μm diameter.[7] In such a case, $P_{cap} < \Delta P_{hyd}$ (assuming channel dimensions as in (a) and ISF viscosity as 0.0035 Pa s),[95] and so ISF will not flow into the channel. However, this can be mitigated in the following ways: i) Increasing channel cross-section area. For example, the channel in section (a) would generate ΔP_{hyd} = 2.6 kPa, but by having a width and height of 500 μm and 1000 μm would generate ΔP_{hyd} = 0.03 kPa, eventually allowing ISF to flow. The same ΔP_{hyd} would be shown by a circular channel of 700 μm diameter. ii) Having an additional pumping source (such as a high osmotic strength hydrogel or vacuum) over the microneedle. Following $\pi_{hydrogel} \gg \pi_{needle} > \pi_{ISF}$ or by interfacing a vacuum chamber (~−50 kPa negative pressure)[81] can facilitate continuous ISF sampling.

7. Sweat and ISF biomarker sensing and quantification in microfluidic platforms

The biomarkers in sweat and ISF inside a microfluidic platform can be quantified *via* multiple sensing principles, the most common ones being colorimetric and electrochemical. Such sensors have been reviewed comprehensively elsewhere[16,22,96] and will only be briefly mentioned here for convenience. Colorimetric and electrochemical sensing techniques are widely used since they are simple to implement and integrate into a microfluidic format. Skin-interfacing microfluidic platforms functioning on colorimetric principles usually include a pre-immobilized biomarker specific assay.[6,31,33,86,89,97–99] The assay uses a solution containing biorecognition molecules, which is introduced in the microchannels either *via* direct addition[33] or through a pre-treated paper.[86] The incoming sweat biomarker reacts with the biorecognition molecules typically undergoing a redox reaction that generates a colored compound (product). The intensity of the color can correlate with the biomarker concentration in sweat. The color intensity of the formed product is commonly measured using smartphone-based image capture and analysis. Their potential downsides may include low sensitivity (~μA mM^{-1}),[100] high limit of detection (LOD, ~mM range), and susceptibility to leaching.

Table 3 Summary of the components of ISF microfluidic devices and their specifications

Device component	RI	Microneedles
Inlet	• $P_{sec} > \Delta P_{hyd}$ necessary • P_{sec} will depend on applied current density	• $P_{osm} \gg P_{needles}$ • $P_{cap} > \Delta P_{hyd}$
Channel dimension	High cross-sectional area and lesser channel length preferred	High cross-sectional area and lesser channel length preferred
Sensor position	Close to inlet	Close to inlet
Outlet	Not necessary	Not necessary

As compared to colorimetric sensors, electrochemical sensors are more sensitive (~nA mM^{-1}), rapidly responsive, remain independent to changes in the background illumination settings, and possess a low LOD (~nM range) and linear dynamic range (LDR). These sensing platforms are mostly built on a three-electrode system – reference, counter, and working. These electrodes can be fabricated *via* photolithography,[101] screen printing,[102] sputter coating,[103] 3-D printing,[39] inkjet printing,[104] wax printing,[105] or direct stamping techniques.[106] They can be printed on sheets of polyimide (PI),[101] polyethylene terephthalate (PET),[107] polyethylene naphthalate (PEN),[48] plastic,[108] polycarbonate (PC),[104] polyester (PE),[109] or tattoo paper.[110] These substrate materials are flexible and easily adhere onto the microfluidic channel. The ink material of the working and counter electrodes ranges between carbon,[107] platinum,[101] silver,[48] and silk.[111] The reference electrode usually comprises Ag/AgCl paste. Sensing is carried out *via* immobilization of a biorecognition element (either enzyme, nanoparticles, antibodies, nucleic acid, or DNA specific to the biomarker) on the working electrode. The biomarkers in the incoming sweat generate a signal (usually a change in current, potential, resistance, or impedance), whose magnitude correlates with the biomarker concentration. The sensitivity of these sensors may be enhanced *via* addition of carbon nanotubes (CNTs), graphene, Pt, or Ag nanoparticles either onto the working electrode surface or mixed with its ink as they increase the electroactive surface area. The next section will provide a brief overview of the common sweat parameters and biomarkers available in sweat and ISF and their physiological relevance.

7.1 Sweat rate analysis

Sweat rate is an important parameter that should be monitored simultaneously with biomarker concentration, as it helps to understand the relationship between biomarker level and sweat volume. Several techniques for evaluating sweat rate in microfluidic platforms have been reported. One involves quantifying sweat rate *via* electrical impedance.[28] This is done by placing two Au electrode fingers on a serpentine microfluidic pathway such that whenever inflowing sweat contacts the electrodes, a change in electrical admittance would occur due to ionic content of sweat. The sweat rate is estimated based on the number of times the admittance value changes due to sweat passage, electrode distance, ionic charge of sweat, and sweat volume. Researchers have also integrated this technique with paper microfluidics, but so far only under *in vitro* settings.[112] Other ways include tracking the progression of colored dyes with sweat inflow.[113] Acoustic field-based resonant sensors have been also integrated in microfluidic channels for sweat rate estimation[114] where the amplitude of the resonant peak determined the sweat rate and ionic concentration. Differences in capacitance generated between two metal plates inside a microfluidic platform with inflow of sweat can help to estimate sweat rate.[115] Additionally, thermistors embedded inside microfluidic channels show a change in resistance upon interfacing flowing sweat.[116] Overall, the sweat rates in impedimetric-based electrochemical microfluidic platforms are commonly measured in conjunction with an electrolyte concentration. This approach is popular because the measured impedance depends on the ionic strength of sweat and the number of times the sweat reaches the impedance electrodes. The electrochemical platforms measuring non-ionic biomarkers mostly do not possess an integrated setup for sweat rate estimation, unlike their colorimetric counterparts. They usually quantify sweat rate using conventional approaches with external tools such as Macroduct® patches, or wicking pads (*via* calculating weight difference before and after the test). Hence, techniques to estimate sweat rate in non-ionic biomarker sensing microfluidic platforms require further development.

7.2 Electrolyte level information

Na^+ and Cl^- are important electrolytes for determining the hydration state of the body. Na^+ and Cl^- ions are the most abundant electrolytes in sweat, whose amount mainly depends on the sweat rate and the reabsorption rate. Dehydration increases the Na^+ concentration in sweat during exercise.[117] Cystic fibrosis (CF) leads to elevated levels of Na^+ and Cl^- in sweat.[118] Usually, the rate of generation of Na^+ and Cl^- is greater than the reabsorption rate during active perspiration. Hence, the concentration of Na^+ and Cl^- increases with exercise.[119] Na^+ and Cl^- ion concentrations in blood can range from 135–150 and 96–106 mM respectively. K^+ in sweat is an indicator of muscle activity and hypo-or hyperkalemic conditions in the body.[23] The sweat potassium concentration ranges within 2–19 mM.[16,119] Na^+, Cl^-, and K^+ in sweat are usually measured using either ion-selective (ISE) membranes, Ag/AgCl electrodes, or PEDOT:PSS electrodes in microfluidic devices.[28,57,59,77,120] ISEs are usually developed inside microfluidic channels for simultaneous detection of multiple electrolytes under active perspiration conditions. Paper microfluidic channels have also been integrated with ISEs and used for sweat electrolyte sensing.[121]

Calcium is an essential biomarker for human metabolism and mineral homeostasis. Excessive levels of calcium in the biofluids can have detrimental effects on the function of organs, which can lead to myeloma, acid–base imbalance, cirrhosis, and renal failure. Ca^{2+} in sweat varies from 0.41 to 12.4 mM.[16] Over the recent years, only a few microfluidic platforms have been developed for sweat Ca^{2+} sensing, but only under active perspiration.[30,35,70] A wearable microfluidic patch used to analyze Ca^{2+} from ISF using selective membranes was reported recently.[7] Electrochemical platforms using Ca^{2+} ionophores have not been yet integrated into microfluidic channels.[122] Hence, further research progress is needed in the microfluidic integration of measuring sweat Ca^{2+}.

7.3 Metabolite information

Lactate is a biomarker for determining the oxidative stress levels and muscle health of the body, and its monitoring is of prime

importance in certain groups of individuals, especially those who are frequently prone to oxygen deficit conditions like athletes and military personnel[100] (for improving training and performance endurance). Several microfluidic platforms have been developed for enzymatic-based sweat lactate sensing, using both colorimetric and electrochemical detection methods. The estimated concentration varies from 10–20 mM, depending on the exercise intensity.[6,29,31,32,34,77,120,123–126] Additionally, since lactate is a conjugate base of lactic acid, its presence is linked with the sweat pH, therefore, lactate sensing patches also need to parallelly monitor sweat pH and skin temperature. The sweat pH and skin temperature are observed to decrease and increase, respectively with increase in sweat lactate content.[57]

Glucose is an important biomarker for diabetes management in the body and is mostly detected in blood *via* the conventional finger pricking test. Hence, the necessity of a wearable platform for continuous sweat glucose monitoring has always been of prime importance. Many researchers have developed microfluidic patches for glucose sensing in sweat.[6,29,31,37,127] The sensing mechanism is usually enzymatic GO_x (glucose oxidase) based, where the enzyme is either immobilized directly into the microfluidic channel (colorimetric),[6,31] or is introduced into the microfluidic pathway (electrochemical).[37] Due to its low levels in sweat, researchers have been more interested in exploring the glucose levels in alternative biological fluids such as interstitial fluid (ISF) using microneedles or reverse iontophoresis (RI), where the amount correlates well with that in blood.[128,129] Ethanol is the biomarker for monitoring intoxication caused by excessive alcohol consumption. Its range in sweat is reported to be between 2.5–25 mM (post 15–40% alcohol drink consumption) and can be sensed electrochemically or colorimetrically detected in microfluidic channels using alcohol oxidase (AO_x) enzyme.[16,23,130,131]

In humans, uric acid (UA) is the major product of the catabolism of purine nucleosides, adenosine, and guanosine and is majorly excreted through kidneys.[132] Uric acid concentration in sweat and blood ranges 2–10 mM (ref. 16) and 5–7 mM, respectively.[23] However, some wearable platforms show a sweat uric acid reading in μM range.[133,134] High uric acid content in the body can be a risk factor for cardiovascular diseases, type 2 diabetes, renal diseases, and gout.[134] Although the mechanism of uric acid partitioning into sweat is not fully understood, it is speculated to occur *via* passive transport to the sweat glands from blood.[135] Only a few microfluidic platforms for uric acid sensing in sweat have been reported. For electrochemical platforms, the sensor is usually interfaced to the microfluidic pathway.[133,134] UA based colorimetric assays have also been immobilized inside microfluidic channels.[33] Even paper microfluidic based UA sensing patches have been developed using plasmonic sensors which are based on label-free surface-enhanced Raman spectroscopy (SERS).[136] Microfluidic-based wearable plasmonic microneedle sensor for minimally invasive ISF uric acid monitoring was reported.[137] Although UA sensing platforms have been developed using different techniques, the concentration discrepancies, and the metabolic process of uric acid partitioning in sweat remains a major unsolved concern, which the microfluidic prototypes to date have not been able to resolve.

Ammonia in sweat has multiple origins like eccrine sweat glands, by-products of urea catabolism, skin gas emissions, and blood plasma.[119] Several studies relate sweat ammonia to fatigue and exercise.[119,138,139] Although multiple platforms quantify sweat ammonia by directly interfacing the skin, few of these are microfluidic based.[131] Ascorbic acid (AA, vitamin C) is present in sweat in the range of 10–50 μM.[16] AA helps in production of collagen, iron absorption, cold treatment, and in protecting the body from viral infections.[140] Microfluidic platforms for detecting sweat AA levels are scarce and are only validated with exercise and exogenous vitamin C intake.[141]

Cortisol is a glucocorticoid, a hormone released in the body to cope with psychological and physiological stresses.[142,143] Sweat cortisol and blood cortisol range between 8–140 ng ml^{-1} and 44–145 ng ml^{-1}, respectively.[16,23,144] Microfluidics means have been used for transporting sweat to the cortisol sensor interface.[142,145] Sensing has been achieved electrochemically using molecular imprinted polymer (MIP) templates, and antibodies in LIG electrodes[142,145] Lateral flow assay (LFA) based platforms for sweat cortisol detection also have been developed on the basis of aptamer conjugated gold nanoparticles (AuNPs).[146] Finally, LFAs for cortisol detection have also been integrated with microfluidic patches.[141]

8. Conclusions: challenges, and prospects of microfluidic sweat and ISF sensors

The application of microfluidics in wearables and point-of-care sensing devices has evolved immensely over the last 10–15 years. This progress began in the latter half of the decade spanning 2000–2010, when researchers started developing in-house microfluidic bioassay platforms for testing of various biological fluids.[147–149] Since 2010, researchers have focused on deploying these platforms for real time on-body sensing applications. Amongst the common biological fluids, sweat and ISF are easy to access and were found to provide a plethora of different biomarkers (similar to many of the ones found in blood). Microfluidic platforms aiming to quantify sweat and ISF biomarkers usually include PDMS/PMMA microfluidic channels, paper channels (chromatography paper and LFA), and thread. The fluid pressure difference between inlet and outlet, capillary forces, surface morphology, and evaporation rate jointly play an important role in controlling the fluid flow through these devices. Moreover, microfluidic valves have also been used for flow regulation in microchannels. The biomarkers are sensed usually using either colorimetry or electrochemical based assays. The bioassay is either positioned directly in the microfluidic channel (for colorimetric sensors) or is interfaced separately onto the microfluidic pathway (common

for electrochemical sensors). The type of sweat and ISF withdrawal technique also determines the sensor location with respect to the device inlet. We discuss such design considerations in section 6. Further elements that will have to be considered when designing such devices are their sustainability and cost.

Sweat rate, pH, glucose, lactate, Na^+, K^+, Ca^{2+}, Cl^-, alcohol, uric acid, ammonia, ascorbic acid, and cortisol have all been monitored with microfluidic devices. Amongst these, microfluidic platforms for Na^+, K^+, Cl^-, lactate, glucose, and alcohol sensing are described in many literature sources. Na^+, K^+, Cl^- appear in sweat and ISF originating from blood, lactate from the muscle fibers, and glucose partially from blood but is mainly found in ISF. On the other hand, microfluidic platforms measuring sweat Ca^{2+}, uric acid, ammonia, ascorbic acid, and cortisol are less common. Consequently, the physiological pathways of these biomarkers in the body are also less well understood based on the data obtained from microfluidic platforms. Electronic integration in a few prototypes has also made possible wireless and real-time biomarker monitoring by wearable devices.

Despite the immense development, there are still certain challenges that microfluidic based sweat sensors need to address (Fig. 6). These challenges are highlighted below:

a. Quantifying the real-time rate of sweat generation is important since it helps to understand the dependency of the biomarker level on the sweat volume. See section 7.1 for a discussion on methods for measuring sweat flow rate. Sweat rate is usually estimated by integrating either impedimetric (measuring frequency of impedance change over time) sensors in the channels[28,53] or by tracking optically the progression of a colored compound in the channels. The first method requires an electrochemical analyzer and has a response time of ~s, while the second method typically uses external hardware (mobile phone, camera) for analysis. Since the colored compound is a product of a chemical reaction, its intensity will rely on the reaction time (usually ~ min) and the external illumination conditions.[31] Overall, as these two techniques are well established, future sweat microfluidic platforms should aim towards adapting similar techniques to estimate sweat rate with the goal of simultaneously determining the effect of sweat rate on the concentration of analyte.

b. Sweat sensors only monitor biochemical levels. To gain comprehensive health information, decisions should be made by simultaneously monitoring biophysical markers (such as heart rate, pulse, SpO_2, core/skin temperature, and blood pressure) as well. Several non-microfluidic prototypes have attempted combining both readouts,[109,150–152] but only one microfluidic prototype has reported heart rate, temperature, and pH with biochemical sensing.[153] Moreover, harvesting and processing the data using advanced machine learning algorithms is necessary to understand the

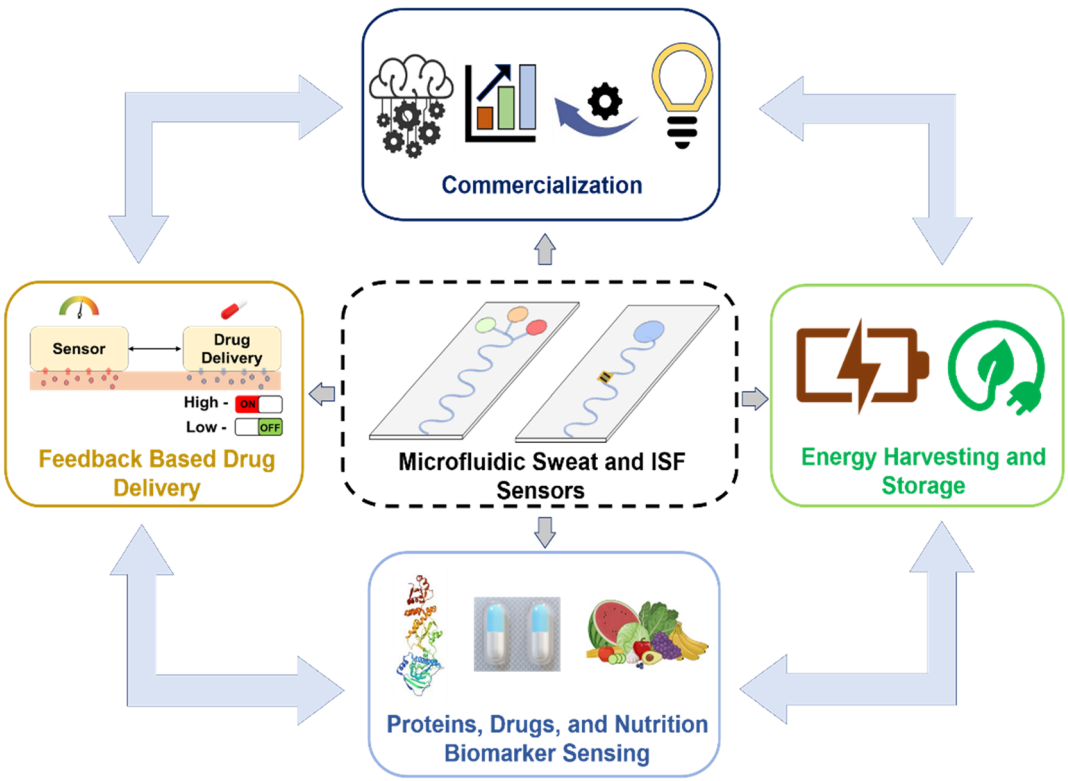

Fig. 6 Summary of some challenges and prospects of sweat and ISF based microfluidic devices. Future research could focus on commercializing more microfluidic platforms, conserving power using BFCs from other sweat biomarkers (except lactate), nutrition sensing from sweat, and sensing the biomarkers which are present in low quantities in sweat.

biomarkers trends over time. This will help in making proactive personalized diagnostic decisions.[154]

c. Commercialized ISF prototypes exist widely for glucose (due to good correlation with blood) and utilize only solid microneedles without microfluidics for sensing.[12] The sensing components in such systems stay functionalized on the needle tips, which makes them susceptible to biofouling or leaching into the skin over time, eventually disrupting their analytical performance. Although commercial microneedles work great (sensing period ~10–14 days), with microfluidic inclusion, the whole sensing module can be setup outside the skin which may enhance the overall performance of such devices.

d. Biochemical sensors often rely on enzymes. Enzymes typically degrade at high pH and temperature. Hence, non-enzymatic (nanozymes) approaches are needed to be developed and integrated.[155,156]

e. Many microfluidic wearable prototypes have only been used on a small number of subjects or without comparison to established standard analytical techniques (such as high-performance liquid chromatography (HPLC) and mass spectrometry). Larger subject validations are needed to justify the accuracy and utility of the device.

f. The power consumption of the microfluidic platforms during sensing needs further minimization. Many microfluidic sensors that support wireless, real-time data monitoring on a mobile device are powered by a commercial Li-ion battery or NFC. Moreover, if the platform extracts sweat or ISF *via* iontophoresis, the power requirement increases further (~mW).[38,61] Furthermore, Li-ion batteries are flammable and sensitive to high temperatures. In preliminary research to address these problems, researchers have started using biofuel cells (BFCs) for harvesting power instead of a battery.[157] A BFC is a fuel cell that uses a catalyst to oxidize its fuel. For sweat based devices, sweat acts as the fuel. However, all established BFCs to date harvest energy only from sweat lactate by directly interfacing the skin because the amount of lactate in sweat is high, and it has a stable generation rate with exercise. Until now, BFCs could only function under exercise (since exercise increases rate of sweat lactate generation), but recently a study showed power harvesting with BFCs without active perspiration.[158] The energy can also be stored in a battery.[159] However, the reported harvested average power can range ~1.2–2 mW from exercise induced sweat[160,161] and ~0.6 mW (ref. 159) during natural perspiration. BFC energy harvesting from ISF has been done using microneedles (power density ~0.4 mW cm^{-2}) and glucose (due to high concentration) but without microfluidics.[162] Thus, microfluidic integration can allow continuous sweat/ISF storage in these BFC patches and on-demand power generation, removing the cumbersome necessity of undergoing physical exertion. Other energy harvesting modalities (such as mechanical or thermal energy) may also be integrated to meet the power requirements of microfluidic platforms.[163,164]

g. Monitoring nutrition related biomarkers (*e.g.*, vitamin C, calcium, Zn, Fe) has attracted attention recently since their amount in the body correlates with skin disorders, digestive complications, bone defects, and even cardiac diseases.[165] However, only a few microfluidic platforms monitor these biomarkers in sweat.[35,97] Hence, new devices are needed for measuring these biomarkers, which should also reveal their physiological pathways. β-Hydroxybutyrate (BHB) is another nutritional biomarker that has recently gained recognition due to its linkage with ketogenic diet and ketoacidosis in type-1 (T1-D) diabetic patients. BHB appears in blood when the body metabolizes fats instead of carbohydrates to produce energy. However, only one (non-microfluidic) sweat based BHB wearable device that operates under active perspiration has been reported.[166] Solid microneedles without microfluidics has also been used for ISF BHB sensing.[167] Based on the increasing popularity of ketogenic diet and its effect on reducing the levels of blood glucose, cholesterol, triglycerides, and body weight,[168] wider application of wearable BHB sensors could be needed.

h. On a similar note, there are no microfluidic platforms available for sensing DNA, neuropeptides, and cytokines from sweat. These biomarkers are present in extremely diluted levels in sweat (~ng ml^{-1} or pg ml^{-1}). However, a few recent studies have shown the continuous monitoring of C-reactive proteins[169] and oestradiol (female hormone)[170] from sweat in microfluidic platforms with IP withdrawn sweat. Continuous and real-time detection of proteins can be achieved with aptamers as the receptor element, but sensitivity will depend on the protein molecular weight, blood-to-ISF lag time, and changes in the local ISF environment.[67,171] Up to date, this concept has been demonstrated with blood[172] and ISF (with microneedles)[173] under a microfluidic setting.

i. Monitoring of drugs in sweat has also received large attention recently, in which levodopa (L-Dopa, a drug for treating Parkinson's disease) has been detected in real human sweat.[52,174] However, the reported prototype for L-Dopa sensing does not involve microfluidics and functions with finger touch based sensing.[52] The partitioning of drugs from blood to sweat is governed by their hydrophobicity and pK_a. Drugs like oxycodone, morphine, and acetaminophen have been detected in sweat with good correlation to plasma levels, but not by using microfluidic tools.[175] Overall, since both IP and osmosis have shown the potential to extract sweat continuously for longer time periods (>24 hours) without exercise,[41,43] integration of microfluidics and IP/osmosis for drug and nutrition metabolite monitoring could provide broader insights regarding their long-term effects. The same concept can even be implemented with microneedles for ISF based sensing.

j. The sweat based microfluidic platforms can be integrated with a feedback-based drug delivery system (similar to an insulin pump). In such systems, whenever the measured biomarker concentration value exceeds its normal level, a drug will be delivered to the body to counter the detrimental effects of the biomarker. The development of such technologies for monitoring multiple biomarkers would contribute strongly towards the development of at-home personalized healthcare. However, the decision regarding the accurate dosage of a drug

should be made by parallelly monitoring other physiological signals such as heart rate, core temperature, sweat pH, and sweat rate.[176] Hence, a multiplexed platform capable of simultaneously monitoring both physiological and biochemical signals in real-time, along with provisions for delivering drugs on demand, can prove useful for this case. Currently, this has been demonstrated only for sweat glucose in a non-microfluidic platform,[177] while solid microneedle based commercial insulin delivery platform (Medtronic MiniMed, CamAPS FX, Control-IQ) exists for ISF glucose.[12]

Overall, the microfluidic sweat and ISF sensing platforms are still in the early stages of development. Future advances can range from constructing a universal sweat rate sensor, including on-demand power generation from sampled biomarkers for running sensing operations, wireless data monitoring *via* electronic integration with cloud storage, making integrated sensors with robust sensing (without external temperature independence), and conducting more clinical studies. To date, only one conventional microfluidic based wearable sweat sensor (for sweat rate, Na^+, and Cl^- detection) has been commercialized after intense clinical validation.[113] Commercial solid microneedle-based ISF sensing platforms for glucose have been developed for continuous glucose monitors.[12,178] However, other generic ISF based microfluidic platforms still remain to be commercialized. Hence, there remain ample opportunities for development of novel microfluidic platforms, wearables, and new modalities for testing in pilot studies and clinical trials with extended monitoring periods for both sweat and ISF.

Author contributions

T. S.: conceptualization, data curation, formal analysis, investigation, validation, writing – original draft, writing – review & editing. S. M.: formal analysis, investigation, validation. M. D. D.: conceptualization, formal analysis, project administration, supervision, validation, writing – review & editing. O. D. V.: conceptualization, formal analysis, project administration, supervision, validation, writing – review & editing.

Conflicts of interest

The authors declare no conflicts of interest.

Acknowledgements

We gratefully acknowledge the support of this study by the US National Science Foundation Nanosystems Engineering Research Center for Advanced Self-Powered Systems of Integrated Sensors and Technologies (ASSIST) (EEC-1160483).

References

1 G. M. Whitesides, *Nature*, 2006, **442**, 368–373.
2 J. Zhang, S. Yan, D. Yuan, G. Alici, N.-T. Nguyen, M. Ebrahimi Warkiani and W. Li, *Lab Chip*, 2016, **16**, 10–34.
3 M. Capanu, J. G. Boyd IV and P. J. Hesketh, *J. Microelectromech. Syst.*, 2000, **9**, 181–189.
4 A. R. Wheeler, W. R. Throndset, R. J. Whelan, A. M. Leach, R. N. Zare, Y. H. Liao, K. Farrell, I. D. Manger and A. Daridon, *Anal. Chem.*, 2003, **75**, 3581–3586.
5 D. J. Beebe, G. A. Mensing and G. M. Walker, *Annu. Rev. Biomed. Eng.*, 2002, **4**, 261–286.
6 A. Koh, D. Kang, Y. Xue, S. Lee, R. M. Pielak, J. Kim, T. Hwang, S. Min, A. Banks, P. Bastien, M. C. Manco, L. Wang, K. R. Ammann, K.-I. Jang, P. Won, S. Han, R. Ghaffari, U. Paik, M. J. Slepian, G. Balooch, Y. Huang and J. A. Rogers, *Sci. Transl. Med.*, 2016, **8**, 366ra165.
7 B. Paul Kunnel and S. Demuru, *Lab Chip*, 2022, **22**, 1793–1804.
8 Y. Zilberman and S. R. Sonkusale, *Biosens. Bioelectron.*, 2015, **67**, 465–471.
9 R. Moreddu, M. Elsherif, H. Adams, D. Moschou, M. F. F. Cordeiro, J. S. S. Wolffsohn, D. Vigolo, H. Butt, J. M. M. Cooper and A. K. K. Yetisen, *Lab Chip*, 2020, **20**, 3970–3979.
10 C. C. Lin, C. C. Tseng, T. K. Chuang, D. S. Lee and G. Bin Lee, *Analyst*, 2011, **136**, 2669–2688.
11 R. Antony, M. S. Giri Nandagopal, N. Sreekumar and N. Selvaraju, *Microsyst. Technol.*, 2014, **20**, 1051–1061.
12 T. Saha, R. Del Caño, K. Mahato, E. De la Paz, C. Chen, S. Ding, L. Yin and J. Wang, *Chem. Rev.*, 2023, **123**, 7854–7889.
13 H. Lim, S. M. Lee, S. Park, C. Choi, H. Kim, J. Kim, M. Mahmood, Y. Lee, J. Kim and W. Yeo, *Biosens. Bioelectron.*, 2022, **210**, 114329.
14 X. Li, C. Zhan, Q. Huang, M. He, C. Yang, C. Yang, X. Huang, M. Chen, X. Xie and H. J. Chen, *ACS Appl. Nano Mater.*, 2022, **5**, 4767–4778.
15 J. Heikenfeld, A. Jajack, B. Feldman, S. W. Granger, S. Gaitonde, G. Begtrup and B. A. Katchman, *Nat. Biotechnol.*, 2019, **37**, 407–419.
16 M. Bariya, H. Y. Y. Nyein and A. Javey, *Nat. Electron.*, 2018, **1**, 160–171.
17 M. Friedel, I. A. P. Thompson, G. Kasting, R. Polsky, D. Cunningham, H. T. Soh and J. Heikenfeld, *Nat. Biomed. Eng.*, 2023, 1–15.
18 L. B. Baker, *Temperature*, 2019, **6**, 211–259.
19 E. De la Paz, T. Saha, R. Del Caño, S. Seker, N. Kshirsagar and J. Wang, *Talanta*, 2023, **254**, 124122.
20 H. Teymourian, F. Tehrani, K. Mahato and J. Wang, *Adv. Healthcare Mater.*, 2021, **10**, 1–19.
21 A. J. Bandodkar, W. J. Jeang, R. Ghaffari and J. A. Rogers, *Annu. Rev. Anal. Chem.*, 2019, **12**, 1–22.
22 J. Min, J. Tu, C. Xu, H. Lukas, S. Shin, Y. Yang, S. A. Solomon, D. Mukasa and W. Gao, *Chem. Rev.*, 2023, **123**, 5049–5138.
23 Z. Sonner, E. Wilder, J. Heikenfeld, G. Kasting, F. Beyette, D. Swaile, F. Sherman, J. Joyce, J. Hagen, N. Kelley-Loughnane and R. Naik, *Biomicrofluidics*, 2015, **9**, 031301.
24 T. D. Wheeler and A. D. Stroock, *Nature*, 2008, **455**, 208–212.
25 T. Saha, R. Del Caño, E. la De Paz, S. S. Sandhu and J. Wang, *Small*, 2022, **2206064**, 2206064.

26 J. Heikenfeld, *Electroanalysis*, 2016, **28**, 1242–1249.
27 S. Ono, G. Egawa and K. Kabashima, *Inflammation Regener.*, 2017, **37**, 1–8.
28 Z. Yuan, L. Hou, M. Bariya, H. Y. Y. Nyein, L. C. Tai, W. Ji, L. Li and A. Javey, *Lab Chip*, 2019, **19**, 3179–3189.
29 A. Martín, J. Kim, J. F. Kurniawan, J. R. Sempionatto, J. R. Moreto, G. Tang, A. S. Campbell, A. Shin, M. Y. Lee, X. Liu and J. Wang, *ACS Sens.*, 2017, **2**, 1860–1868.
30 X. He, T. Xu, Z. Gu, W. Gao, L. P. Xu, T. Pan and X. Zhang, *Anal. Chem.*, 2019, **91**, 4296–4300.
31 J. Choi, A. J. Bandodkar, J. T. Reeder, T. R. Ray, A. Turnquist, S. B. Kim, N. Nyberg, A. Hourlier-Fargette, J. B. Model, A. J. Aranyosi, S. Xu, R. Ghaffari and J. A. Rogers, *ACS Sens.*, 2019, **4**, 379–388.
32 A. J. Bandodkar, P. Gutruf, J. Choi, K. Lee, Y. Sekine, J. T. Reeder, W. J. Jeang, A. J. Aranyosi, S. P. Lee, J. B. Model, R. Ghaffari, C.-J. Su, J. P. Leshock, T. Ray, A. Verrillo, K. Thomas, V. Krishnamurthi, S. Han, J. Kim, S. Krishnan, T. Hang and J. A. Rogers, *Sci. Adv.*, 2019, **5**, eaav3294.
33 Y. Zhang, H. Guo, S. B. Kim, Y. Wu, D. Ostojich, S. H. Park, X. Wang, Z. Weng, R. Li, A. J. Bandodkar, Y. Sekine, J. Choi, S. Xu, S. Quaggin, R. Ghaffari and J. A. Rogers, *Lab Chip*, 2019, **19**, 1545–1555.
34 J. Choi, D. Kang, S. Han, S. B. Kim and J. A. Rogers, *Adv. Healthcare Mater.*, 2017, **6**, 1601355.
35 J. Kim, Y. Wu, H. Luan, D. S. Yang, D. Cho, S. S. Kwak, S. Liu, H. Ryu, R. Ghaffari and J. A. Rogers, *Adv. Sci.*, 2022, **9**, 2103331.
36 M. Herrero-Fernandez, T. Montero-Vilchez, P. Diaz-Calvillo, M. Romera-Vilchez, A. Buendia-Eisman and S. Arias-Santiago, *J. Clin. Med.*, 2022, **11**, 298.
37 G. Bolat, E. De la Paz, N. F. Azeredo, M. Kartolo, J. Kim, A. N. de Loyola e Silva, R. Rueda, C. Brown, L. Angnes, J. Wang and J. R. Sempionatto, *Anal. Bioanal. Chem.*, 2022, **414**, 5411–5421.
38 J. Kim, J. R. Sempionatto, S. Imani, M. C. Hartel, A. Barfidokht, G. Tang, A. S. Campbell, P. P. Mercier, J. Wang, J. Kim, J. R. Sempionatto, M. C. Hartel, A. Barfidokht, G. Tang, A. S. Campbell, J. Wang, S. Imani and P. P. Mercier, *Adv. Sci.*, 2018, **5**, 1800880.
39 Y. Song, R. Y. Tay, J. Li, C. Xu, J. Min, E. Shirzaei Sani, G. Kim, W. Heng, I. Kim and W. Gao, *Sci. Adv.*, 2023, **9**, 1–14.
40 S. Li, K. Hart, N. Norton, C. A. Ryan, L. Guglani and M. R. Prausnitz, *Bioeng. Transl. Med.*, 2021, **6**, 1–9.
41 P. Simmers, S. K. Li, G. Kasting and J. Heikenfeld, *J. Dermatol. Sci.*, 2018, **89**, 40–51.
42 M. Roustit, S. Blaise and J. L. Cracowski, *Br. J. Clin. Pharmacol.*, 2014, **77**, 63–71.
43 T. Saha, J. Fang, S. Mukherjee, M. D. Dickey and O. D. Velev, *ACS Appl. Mater. Interfaces*, 2021, **13**, 8071–8081.
44 T. Saha, J. Fang, S. Mukherjee, C. T. Knisely, M. D. Dickey and O. D. Velev, *Micromachines*, 2021, **12**, 1513.
45 T. Saha, J. Fang, M. A. Yokus, S. Mukherjee, A. Bozkurt, M. A. Daniele, M. D. Dickey and O. D. Velev, in *2021 43rd Annual International Conference of the IEEE Engineering in Medicine & Biology Society (EMBC)*, IEEE, 2021, vol. 13, pp. 6863–6866.
46 M. A. Yokus, T. Saha, J. Fang, M. D. Dickey, O. D. Velev and M. A. Daniele, in *2019 IEEE SENSORS*, IEEE, 2019, vol. 2019, pp. 1–4.
47 T. Shay, M. D. Dickey and O. D. Velev, *Lab Chip*, 2017, **17**, 710–716.
48 K. Nagamine, T. Mano, A. Nomura, Y. Ichimura, R. Izawa, H. Furusawa, H. Matsui, D. Kumaki and S. Tokito, *Sci. Rep.*, 2019, **9**, 1–8.
49 G. S. Liu, Y. Kong, Y. Wang, Y. Luo, X. Fan, X. Xie, B. R. Yang and M. X. Wu, *Biomaterials*, 2020, **232**, 119740.
50 S. Lin, B. Wang, Y. Zhao, R. Shih, X. Cheng, W. Yu, H. Hojaiji, H. Lin, C. Hoffman, D. Ly, J. Tan, Y. Chen, D. Di Carlo, C. Milla and S. Emaminejad, *ACS Sens.*, 2020, **5**, 93–102.
51 J. R. R. Sempionatto, J. M. J.-M. Moon and J. Wang, *ACS Sens.*, 2021, **6**, 1875–1883.
52 J. Moon, H. Teymourian, E. De la Paz, J. R. Sempionatto, K. Mahato, T. Sonsa-ard, N. Huang, K. Longardner, I. Litvan and J. Wang, *Angew. Chem., Int. Ed.*, 2021, **60**, 19074–19078.
53 H. Y. Y. Nyein, M. Bariya, B. Tran, C. H. Ahn, B. J. Brown, W. Ji, N. Davis and A. Javey, *Nat. Commun.*, 2021, **12**, 1–13.
54 W. Tang, L. Yin, J. R. Sempionatto, J. Moon, H. Teymourian and J. Wang, *Adv. Mater.*, 2021, **33**, 2008465.
55 M. Bariya, L. Li, R. Ghattamaneni, C. H. Ahn, H. Y. Y. Nyein, L.-C. Tai and A. Javey, *Sci. Adv.*, 2020, **6**, 1–10.
56 N. A. S. Taylor and C. A. Machado-Moreira, *Extreme Physiol. Med.*, 2013, **2**, 4.
57 W. Gao, S. Emaminejad, H. Y. Y. Nyein, S. Challa, K. Chen, A. Peck, H. M. Fahad, H. Ota, H. Shiraki, D. Kiriya, D.-H. H. Lien, G. A. Brooks, R. W. Davis and A. Javey, *Nature*, 2016, **529**, 509–514.
58 S. Emaminejad, W. Gao, E. Wu, Z. A. Davies, H. Yin Yin Nyein, S. Challa, S. P. Ryan, H. M. Fahad, K. Chen, Z. Shahpar, S. Talebi, C. Milla, A. Javey and R. W. Davis, *Proc. Natl. Acad. Sci. U. S. A.*, 2017, **114**, 4625–4630.
59 H. Y. Y. Nyein, L. C. Tai, Q. P. Ngo, M. Chao, G. B. Zhang, W. Gao, M. Bariya, J. Bullock, H. Kim, H. M. Fahad and A. Javey, *ACS Sens.*, 2018, **3**, 944–952.
60 M. Wang, Y. Yang, J. Min, Y. Song, J. Tu, D. Mukasa, C. Ye, C. Xu, N. Heflin, J. S. McCune, T. K. Hsiai, Z. Li and W. Gao, *Nat. Biomed. Eng.*, 2022, **6**, 1225–1235.
61 T. Saha, T. Songkakul, C. T. Knisely, M. A. Yokus, M. A. Daniele, M. D. Dickey, A. Bozkurt and O. D. Velev, *ACS Sens.*, 2022, **7**, 2037–2048.
62 H. Zheng, Z. Pu, H. Wu, C. Li, X. Zhang and D. Li, *Biosens. Bioelectron.*, 2023, **223**, 115036.
63 L. K. Vora, A. H. Sabri, P. E. McKenna, A. Himawan, A. R. J. Hutton, U. Detamornrat, A. J. Paredes, E. Larrañeta and R. F. Donnelly, *Nat. Rev. Bioeng.*, 2023, DOI: **10.1038/s44222-023-00108-7**.
64 K. M. Saifullah and Z. Faraji Rad, *Adv. Mater. Interfaces*, 2023, **10**, 1–22.
65 F. Tehrani, H. Teymourian, B. Wuerstle, J. Kavner, R. Patel, A. Furmidge, R. Aghavali, H. Hosseini-Toudeshki, C. Brown, F. Zhang, K. Mahato, Z. Li, A. Barfidokht, L. Yin, P. Warren, N. Huang, Z. Patel, P. P. Mercier and J. Wang, *Nat. Biomed. Eng.*, 2022, **6**, 1214–1224.

66 P. R. Miller, R. M. Taylor, B. Q. Tran, G. Boyd, T. Glaros, V. H. Chavez, R. Krishnakumar, A. Sinha, K. Poorey, K. P. Williams, S. S. Branda, J. T. Baca and R. Polsky, *Commun. Biol.*, 2018, **1**, 173.
67 T. Young, V. Clark, N. Arroyo-Currás and J. Heikenfeld, *ECS Sens. Plus*, 2023, **2**, 027001.
68 M. J. Fuerstman, A. Lai, M. E. Thurlow, S. S. Shevkoplyas, H. A. Stone and G. M. Whitesides, *Lab Chip*, 2007, **7**, 1479–1489.
69 N. B. Twine, R. M. Norton, M. C. Brothers, A. Hauke, E. F. Gomez and J. Heikenfeld, *Lab Chip*, 2018, **18**, 2816–2825.
70 M. R. Ely, B. R. Ely, T. D. Chinevere, C. P. Lacher, H. C. Lukaski and S. N. Cheuvront, *Physiol. Meas.*, 2012, **33**, 385–394.
71 G. Matzeu, C. Fay, A. Vaillant, S. Coyle and D. Diamond, *IEEE Trans. Biomed. Eng.*, 2016, **63**, 1672–1680.
72 A. M. Nightingale, C. L. Leong, R. A. Burnish, S. ul Hassan, Y. Zhang, G. F. Clough, M. G. Boutelle, D. Voegeli and X. Niu, *Nat. Commun.*, 2019, **10**, 1–12.
73 A. Gonzalez, L. Estala, M. Gaines and F. A. Gomez, *Electrophoresis*, 2016, **37**, 1685–1690.
74 J. Son, G. Y. Bae, S. Lee, G. Lee, S. W. Kim, D. Kim, S. Chung and K. Cho, *Adv. Mater.*, 2021, **33**, 2102740.
75 C. W. Bae, P. T. Toi, B. Y. Kim, W. Il Lee, H. B. Lee, A. Hanif, E. H. Lee and N. E. Lee, *ACS Appl. Mater. Interfaces*, 2019, **11**, 14567–14575.
76 A. Cazalé, W. Sant, F. Ginot, J.-C. Launay, G. Savourey, F. Revol-Cavalier, J. M. Lagarde, D. Heinry, J. Launay and P. Temple-Boyer, *Sens. Actuators, B*, 2016, **225**, 1–9.
77 S. Anastasova, B. Crewther, P. Bembnowicz, V. Curto, H. M. Ip, B. Rosa and G.-Z. Z. Yang, *Biosens. Bioelectron.*, 2017, **93**, 139–145.
78 Z. Nie, C. A. Nijhuis, J. Gong, X. Chen, A. Kumachev, A. W. Martinez, M. Narovlyansky and G. M. Whitesides, *Lab Chip*, 2010, **10**, 477–483.
79 S. G. Jeong, J. Kim, S. H. Jin, K. S. Park and C. S. Lee, *Korean J. Chem. Eng.*, 2016, **33**, 2761–2770.
80 C. C. Tseng, C. Te Kung, R. F. Chen, M. H. Tsai, H. R. Chao, Y. N. Wang and L. M. Fu, *Sens. Actuators, B*, 2021, **342**, 130078.
81 T. Abbasiasl, F. Mirlou, H. Mirzajani, M. J. Bathaei, E. Istif, N. Shomalizadeh, R. E. Cebecioğlu, E. E. Özkahraman, U. C. Yener and L. Beker, *Adv. Mater.*, 2023, **2304704**, 1–17.
82 J. Yang, R. Luo, L. Yang, X. Wang and Y. Huang, *Int. J. Mol. Sci.*, 2023, **24**, 9882.
83 H. Cho, H. Y. Kim, J. Y. Kang and T. S. Kim, *J. Colloid Interface Sci.*, 2007, **306**, 379–385.
84 N. Mishra, N. T. Garland, K. A. Hewett, M. Shamsi, M. D. Dickey and A. J. Bandodkar, *ACS Sens.*, 2022, **7**, 3169–3180.
85 H. Zhang, Y. Qiu, S. Yu, C. Ding, J. Hu, H. Qi, Y. Tian, Z. Zhang, A. Liu and H. Wu, *Biomicrofluidics*, 2022, **16**, 044104.
86 A. J. Bandodkar, J. Choi, S. P. Lee, W. J. Jeang, P. Agyare, P. Gutruf, S. Wang, R. A. Sponenburg, J. T. Reeder, S. Schon, T. R. Ray, S. Chen, S. Mehta, S. Ruiz and J. A. Rogers, *Adv. Mater.*, 2019, **31**, 1902109.
87 H. Lin, J. Tan, J. Zhu, S. Lin, Y. Zhao, W. Yu, H. Hojaiji, B. Wang, S. Yang, X. Cheng, Z. Wang, E. Tang, C. Yeung and S. Emaminejad, *Nat. Commun.*, 2020, **11**, 4405.
88 J. Xiao, Y. Liu, L. Su, D. Zhao, L. Zhao and X. Zhang, *Anal. Chem.*, 2019, **91**, 14803–14807.
89 J. T. Reeder, J. Choi, Y. Xue, P. Gutruf, J. Hanson, M. Liu, T. Ray, A. J. Bandodkar, R. Avila, W. Xia, S. Krishnan, S. Xu, K. Barnes, M. Pahnke, R. Ghaffari, Y. Huang and J. A. Rogers, *Sci. Adv.*, 2019, **5**, eaau6356.
90 J. Choi, S. Chen, Y. Deng, Y. Xue, J. T. Reeder, D. Franklin, Y. S. Oh, J. B. Model, A. J. Aranyosi, S. P. Lee, R. Ghaffari, Y. Huang and J. A. Rogers, *Adv. Healthcare Mater.*, 2021, **10**, 2000722.
91 T. Shay, T. Saha, M. D. Dickey and O. D. Velev, *Biomicrofluidics*, 2020, **14**, 034112.
92 A. R. Naik, Y. Zhou, A. A. Dey, D. L. G. Arellano, U. Okoroanyanwu, E. B. Secor, M. C. Hersam, J. Morse, J. P. Rothstein, K. R. Carter and J. J. Watkins, *Lab Chip*, 2022, **22**, 156–169.
93 H. B. Lee, M. Meeseepong, T. Q. Trung, B. Y. Kim and N. E. Lee, *Biosens. Bioelectron.*, 2020, **156**, 112133.
94 P. Bacchin, J. Leng and J. B. Salmon, *Chem. Rev.*, 2022, **122**, 6938–6985.
95 K. Takeuchi, N. Takama, K. Sharma, O. Paul, P. Ruther, T. Suga and B. Kim, *Drug Delivery Transl. Res.*, 2022, **12**, 435–443.
96 K. M. Clark and T. R. Ray, *ACS Sens.*, 2023, **8**, 3606–3622.
97 Y. Sekine, S. B. Kim, Y. Zhang, A. J. Bandodkar, S. Xu, J. Choi, M. Irie, T. R. Ray, P. Kohli, N. Kozai, T. Sugita, Y. Wu, K. Lee, K.-T. Lee, R. Ghaffari and J. A. Rogers, *Lab Chip*, 2018, **18**, 2178–2186.
98 T. R. Ray, J. Choi, A. J. Bandodkar, S. Krishnan, P. Gutruf, L. Tian, R. Ghaffari and J. A. Rogers, *Chem. Rev.*, 2019, **119**, 5461–5533.
99 S. B. Kim, Y. Zhang, S. M. Won, A. J. Bandodkar, Y. Sekine, Y. Xue, J. Koo, S. W. Harshman, J. A. Martin, J. M. Park, T. R. Ray, K. E. Crawford, K. Lee, J. Choi, R. L. Pitsch, C. C. Grigsby, A. J. Strang, Y. Chen, S. Xu, J. Kim, A. Koh, J. S. Ha, Y. Huang, S. W. Kim and J. A. Rogers, *Small*, 2018, **14**, 1703334.
100 F. Alam, S. RoyChoudhury, A. H. Jalal, Y. Umasankar, S. Forouzanfar, N. Akter, S. Bhansali and N. Pala, *Biosens. Bioelectron.*, 2018, **117**, 818–829.
101 B. K. Ashley, M. S. Brown, Y. Park, S. Kuan and A. Koh, *Biosens. Bioelectron.*, 2019, **132**, 343–351.
102 M. E. Payne, A. Zamarayeva, V. I. Pister, N. A. D. Yamamoto and A. C. Arias, *Sci. Rep.*, 2019, **9**, 1–10.
103 C. Meyerhoff, F. Bischof, F. J. Mennel, F. Sternberg, J. Bican and E. F. Pfeiffer, *Biosens. Bioelectron.*, 1993, **8**, 409–414.
104 E. L. Tur-García, F. Davis, S. D. Collyer, J. L. Holmes, H. Barr and S. P. J. Higson, *Sens. Actuators, B*, 2017, **242**, 502–510.
105 Z. Nie, F. Deiss, X. Liu, O. Akbulut and G. M. Whitesides, *Lab Chip*, 2010, **10**, 3163.
106 M. A. Abrar, Y. Dong, P. K. Lee and W. S. Kim, *Sci. Rep.*, 2016, **6**, 30565.
107 K. Enomoto, R. Shimizu and H. Kudo, *Electron. Commun. Jpn.*, 2018, **101**, 41–46.

108 M. Onor, S. Gufoni, T. Lomonaco, S. Ghimenti, P. Salvo, F. Sorrentino and E. Bramanti, *Anal. Chim. Acta*, 2017, **989**, 80–87.
109 S. Imani, A. J. Bandodkar, A. M. V. Mohan, R. Kumar, S. Yu, J. Wang and P. P. Mercier, *Nat. Commun.*, 2016, **7**, 11650.
110 W. Jia, A. J. Bandodkar, G. Valdés-Ramírez, J. R. Windmiller, Z. Yang, J. Ramírez, G. Chan and J. Wang, *Anal. Chem.*, 2013, **85**, 6553–6560.
111 W. He, C. Wang, H. Wang, M. Jian, W. Lu, X. Liang, X. Zhang, F. Yang and Y. Zhang, *Sci. Adv.*, 2019, **5**, eaax0649.
112 M. A. Yokus, T. Agcayazi, M. Traenkle, A. Bozkurt and M. A. Daniele, in *2020 IEEE SENSORS*, IEEE, 2020, vol. 2020-Octob, 14–17.
113 L. B. Baker, J. B. Model, K. A. Barnes, M. L. Anderson, S. P. Lee, K. A. Lee, S. D. Brown, A. J. Reimel, T. J. Roberts, R. P. Nuccio, J. L. Bonsignore, C. T. Ungaro, J. M. Carter, W. Li, M. S. Seib, J. T. Reeder, A. J. Aranyosi, J. A. Rogers and R. Ghaffari, *Sci. Adv.*, 2020, **6**, 17–19.
114 A. R. Carr, Y. H. Patel, C. R. Neff, S. Charkhabi, N. E. Kallmyer, H. F. Angus and N. F. Reuel, *NPJ Digit. Med.*, 2020, **3**, 62.
115 D. H. Choi, M. Gonzales, G. B. Kitchen, D. T. Phan and P. C. Searson, *ACS Sens.*, 2020, **5**, 3821–3826.
116 K. Kwon, J. U. Kim, Y. Deng, S. R. Krishnan, J. Choi, H. Jang, K. Lee, C.-J. Su, I. Yoo, Y. Wu, L. Lipschultz, J.-H. Kim, T. S. Chung, D. Wu, Y. Park, T. Kim, R. Ghaffari, S. Lee, Y. Huang and J. A. Rogers, *Nat. Electron.*, 2021, **4**, 302–312.
117 B. Schazmann, D. Morris, C. Slater, S. Beirne, C. Fay, R. Reuveny, N. Moyna and D. Diamond, *Anal. Methods*, 2010, **2**, 342–348.
118 M. B. Brown, N. A. McCarty and M. Millard-Stafford, *Am. J. Physiol.*, 2011, **301**, 1177–1185.
119 L. Klous, C. J. de Ruiter, S. Scherrer, N. Gerrett and H. A. M. Daanen, *Eur. J. Appl. Physiol.*, 2021, **121**, 803–816.
120 R. Vinoth, T. Nakagawa, J. Mathiyarasu and A. M. V. Mohan, *ACS Sens.*, 2021, **6**, 1174–1186.
121 B. Liang, Q. Cao, L. Fang, X. Mao, T. Tu, X. Ye, W. Pan, T. Tu, L. Fang and X. Ye, in *2019 IEEE SENSORS*, IEEE, 2019, vol. 21, pp. 1–4.
122 H. Y. Y. Nyein, W. Gao, Z. Shahpar, S. Emaminejad, S. Challa, K. Chen, H. M. Fahad, L. C. Tai, H. Ota, R. W. Davis and A. Javey, *ACS Nano*, 2016, **10**, 7216–7224.
123 G. Xiao, J. He, Y. Qiao, F. Wang, Q. Xia, X. Wang, L. Yu, Z. Lu and C.-M. Li, *Adv. Fiber Mater.*, 2020, **2**, 265–278.
124 X. Xuan, C. Pérez-Ràfols, C. Chen, M. Cuartero and G. A. Crespo, *ACS Sens.*, 2021, **6**, 2763–2771.
125 F. Poletti, B. Zanfrognini, L. Favaretto, V. Quintano, J. Sun, E. Treossi, M. Melucci, V. Palermo and C. Zanardi, *Sens. Actuators, B*, 2021, **344**, 130253.
126 M. Li, L. Wang, R. Liu, J. Li, Q. Zhang, G. Shi, Y. Li, C. Hou and H. Wang, *Biosens. Bioelectron.*, 2021, **174**, 112828.
127 H. Hojaiji, Y. Zhao, M. C. Gong, M. Mallajosyula, J. Tan, H. Lin, A. M. Hojaiji, S. Lin, C. Milla, A. M. Madni and S. Emaminejad, *Lab Chip*, 2020, **20**, 4582–4591.
128 J. Zhu, X. Zhou, H. J. Kim, M. Qu, X. Jiang, K. J. Lee, L. Ren, Q. Wu, C. Wang, X. Zhu, P. Tebon, S. Zhang, J. Lee, N. Ashammakhi, S. Ahadian, M. R. Dokmeci, Z. Gu, W. Sun and A. Khademhosseini, *Small*, 2020, **16**, 1–9.
129 E. De la Paz, A. Barfidokht, S. Rios, C. Brown, E. Chao and J. Wang, *Anal. Chem.*, 2021, **93**, 12767–12775.
130 A. Hauke, P. Simmers, Y. R. Ojha, B. D. Cameron, R. Ballweg, T. Zhang, N. Twine, M. Brothers, E. Gomez and J. Heikenfeld, *Lab Chip*, 2018, **18**, 3750–3759.
131 S. B. Kim, J. Koo, J. Yoon, A. Hourlier-Fargette, B. Lee, S. Chen, S. Jo, J. Choi, Y. S. Oh, G. Lee, S. M. Won, A. J. Aranyosi, S. P. Lee, J. B. Model, P. V. Braun, R. Ghaffari, C. Park and J. A. Rogers, *Lab Chip*, 2020, **20**, 84–92.
132 C. C. T. C. Huang, M. M. L. M. Chen, L. L. L. Huang and I. F. I. Mao, *Chin. J. Physiol.*, 2002, **45**, 109–115.
133 Z. Xu, J. Song, B. Liu, S. Lv and F. Gao, *Sens. Actuators, B*, 2021, **348**, 130674.
134 Y. Yang, Y. Song, X. Bo, J. Min, O. S. Pak, L. Zhu, M. Wang, J. Tu, A. Kogan, H. Zhang, T. K. Hsiai, Z. Li and W. Gao, *Nat. Biotechnol.*, 2020, **38**, 217–224.
135 G. K. Komives, S. Robinson and J. T. Roberts, *J. Appl. Physiol.*, 1966, **21**, 1681–1684.
136 U. Mogera, H. Guo, M. Namkoong, M. S. Rahman, T. Nguyen and L. Tian, *Sci. Adv.*, 2022, **8**, 1–12.
137 J. Xiao, S. Zhang, Q. Liu, T. Xu and X. Zhang, *Sens. Actuators, B*, 2024, **398**, 134685.
138 F. Meyer, O. Laitano, O. Bar-Or, D. McDougall and G. J. F. Heigenhauser, *Braz. J. Med. Biol. Res.*, 2007, **40**, 135–143.
139 W. Ament, J. Huizenga, G. Mook, C. Gips and C. J. Verkerke, *Int. J. Sports Med.*, 1997, **18**, 35–39.
140 J. R. Sempionatto, A. A. Khorshed, A. Ahmed, A. N. De Loyola E Silva, A. Barfidokht, L. Yin, K. Y. Goud, M. A. Mohamed, E. Bailey, J. May, C. Aebischer, C. Chatelle and J. Wang, *ACS Sens.*, 2020, **5**, 1804–1813.
141 S. Kim, B. Lee, J. T. Reeder, S. H. Seo, S. U. Lee, A. Hourlier-Fargette, J. Shin, Y. Sekine, H. Jeong, Y. S. Oh, A. J. Aranyosi, S. P. Lee, J. B. Model, G. Lee, M. H. Seo, S. S. Kwak, S. Jo, G. Park, S. Han, I. Park, H. Il Jung, R. Ghaffari, J. Koo, P. V. Braun and J. A. Rogers, *Proc. Natl. Acad. Sci. U. S. A.*, 2020, **117**, 27906–27915.
142 R. M. Torrente-Rodríguez, J. Tu, Y. Yang, J. Min, M. Wang, Y. Song, Y. Yu, C. Xu, C. Ye, W. W. IsHak and W. Gao, *Matter*, 2020, **2**, 921–937.
143 D. Kinnamon, R. Ghanta, K. C. Lin, S. Muthukumar and S. Prasad, *Sci. Rep.*, 2017, **7**, 1–13.
144 M. Zea, F. G. Bellagambi, H. Ben Halima, N. Zine, N. Jaffrezic-Renault, R. Villa, G. Gabriel and A. Errachid, *TrAC, Trends Anal. Chem.*, 2020, **132**, 116058.
145 O. Parlak, S. T. Keene, A. Marais, V. F. Curto and A. Salleo, *Sci. Adv.*, 2018, **4**, eaar2904.
146 S. Dalirirad and A. J. Steckl, *Sens. Actuators, B*, 2019, 79–86.
147 A. W. Martinez, S. T. Phillips, E. Carrilho, S. W. Thomas, H. Sindi and G. M. Whitesides, *Anal. Chem.*, 2008, **80**, 3699–3707.
148 A. W. Martinez, S. T. Phillips, M. J. Butte and G. M. Whitesides, *Angew. Chem., Int. Ed.*, 2007, **46**, 1318–1320.
149 A. W. Martinez, S. T. Phillips, Z. Nie, C. M. Cheng, E. Carrilho, B. J. Wiley and G. M. Whitesides, *Lab Chip*, 2010, **10**, 2499–2504.

150 J. R. Sempionatto, M. Lin, L. Yin, E. De la Paz, K. Pei, T. Sonsa-Ard, A. N. de Loyola Silva, A. A. Khorshed, F. Zhang, N. Tostado, S. Xu and J. Wang, *Nat. Biomed. Eng.*, 2021, **5**, 737–748.
151 Y. Xu, E. De la Paz, A. Paul, K. Mahato, J. R. Sempionatto, N. Tostado, M. Lee, G. Hota, M. Lin, A. Uppal, W. Chen, S. Dua, L. Yin, B. L. Wuerstle, S. Deiss, P. Mercier, S. Xu, J. Wang and G. Cauwenberghs, *Nat. Biomed. Eng.*, 2023, **7**, 1307–1320.
152 Y. J. Hong, H. Lee, J. Kim, M. Lee, H. J. Choi, T. Hyeon and D. H. Kim, *Adv. Funct. Mater.*, 2018, **28**, 1–12.
153 T. Li, B. Liang, Z. Ye, L. Zhang, S. Xu, T. Tu, Y. Zhang, Y. Cai, B. Zhang, L. Fang, X. Mao, S. Zhang, G. Wu, Q. Yang, C. Zhou, X. Cai and X. Ye, *Biosens. Bioelectron.*, 2022, **198**, 113855.
154 C. Chen, S. Ding and J. Wang, *Nat. Med.*, 2023, **29**, 1623–1630.
155 A. Tripathi, K. D. Harris and A. L. Elias, *ACS Omega*, 2020, **5**, 9123–9130.
156 A. Tripathi, K. D. Harris and A. L. Elias, *PLoS One*, 2021, **16**, e0257777.
157 Y. Yu, J. Nassar, C. Xu, J. Min, Y. Yang, A. Dai, R. Doshi, A. Huang, Y. Song, R. Gehlhar, A. D. Ames and W. Gao, *Sci. Robot.*, 2020, **5**, 1–14.
158 L. Yin, J. Moon, R. Sempionatto, S. Xu, J. Wang, L. Yin, J. Moon, J. R. Sempionatto, M. Lin, M. Cao, A. Trifonov, F. Zhang, Z. Lou, J. Jeong, S. Lee and S. Xu, *Joule*, 2021, **5**, 1888–1904.
159 L. Yin, M. Cao, K. N. Kim, M. Lin, J.-M. M. Moon, J. R. Sempionatto, J. Yu, R. Liu, C. Wicker, A. Trifonov, F. Zhang, H. Hu, J. R. Moreto, J. Go, S. Xu and J. Wang, *Nat. Electron.*, 2022, **5**, 694–705.
160 A. J. Bandodkar, J.-M. You, N.-H. Kim, Y. Gu, R. Kumar, A. M. V. Mohan, J. Kurniawan, S. Imani, T. Nakagawa, B. Parish, M. Parthasarathy, P. P. Mercier, S. Xu and J. Wang, *Energy Environ. Sci.*, 2017, **10**, 1581–1589.
161 L. Yin, S. S. Sandhu, R. Liu, M. I. Khan, C. Wicker, V. Garcia-Gradilla, J. Zhou, A. Chang, S. Wu, J. Moon, C. Chen, S. Ding and J. Wang, *Adv. Energy Mater.*, 2023, **13**, 1–11.
162 S. Kusama, K. Sato, Y. Matsui, N. Kimura, H. Abe, S. Yoshida and M. Nishizawa, *Nat. Commun.*, 2021, **12**, 658.
163 V. Vallem, Y. Sargolzaeiaval, M. Ozturk, Y. C. Lai and M. D. Dickey, *Adv. Mater.*, 2021, **33**, 1–37.
164 V. Padmanabhan Ramesh, Y. Sargolzaeiaval, T. Neumann, V. Misra, D. Vashaee, M. D. Dickey and M. C. Ozturk, *npj Flexible Electron.*, 2021, **5**, 5.
165 T. M. Cascino and S. L. Hummel, *J. Am. Heart Assoc.*, 2018, **7**, 1–3.
166 X. Zhang, Y. Xia, Y. Liu, S. M. Mugo and Q. Zhang, *Anal. Chem.*, 2022, **94**, 993–1002.
167 S. Alva, K. Castorino, H. Cho and J. Ou, *J. Diabetes Sci. Technol.*, 2021, **15**, 768–774.
168 H. M. Dashti, T. C. Mathew, T. Hussein, S. K. Asfar, A. Behbahani, M. A. Khoursheed, H. M. Al-Sayer, Y. Y. Bo-Abbas and N. S. Al-Zaid, *Exp. Clin. Cardiol.*, 2004, **9**, 200–205.
169 J. Tu, J. Min, Y. Song, C. Xu, J. Li, J. Moore, J. Hanson, E. Hu, T. Parimon, T. Wang, E. Davoodi, T. Chou, P. Chen, J. J. Hsu, H. B. Rossiter and W. Gao, *Nat. Biomed. Eng.*, 2023, **7**, 1293–1306.
170 C. Ye, M. Wang, J. Min, R. Y. Tay, H. Lukas, J. R. Sempionatto, J. Li, C. Xu and W. Gao, *Nat. Nanotechnol.*, 2023, DOI: **10.1038/s41565-023-01513-0**.
171 C. Parolo, A. Idili, J. Heikenfeld and K. W. Plaxco, *Lab Chip*, 2023, **23**, 1339–1348.
172 B. S. Ferguson, D. A. Hoggarth, D. Maliniak, K. Ploense, R. J. White, N. Woodward, K. Hsieh, A. J. Bonham, M. Eisenstein, T. E. Kippin, K. W. Plaxco and H. T. Soh, *Sci. Transl. Med.*, 2013, **5**, 213ra165.
173 M. Friedel, B. Werbovetz, A. Drexelius, Z. Watkins, A. Bali, K. W. Plaxco and J. Heikenfeld, *Lab Chip*, 2023, **23**, 3289–3299.
174 H. C. Ates, P. Q. Nguyen, L. Gonzalez-Macia, E. Morales-Narváez, F. Güder, J. J. Collins and C. Dincer, *Nat. Rev. Mater.*, 2022, **15**, 1–23.
175 T. Ruwe, E. White, A. S. Zebertavage, D. Runnoe, D. Fay, H. Daumeyer, T. S. Tracy, K. F. Uchtman, G. Begtrup, Y. Yuan, J. Heikenfeld and W. A. Buggele, *Ther. Drug Monit.*, 2023, **45**, 731–742.
176 S. Xu, J. Kim, J. R. Walter, R. Ghaffari and J. A. Rogers, *Sci. Transl. Med.*, 2022, **14**, eabn6036.
177 H. Lee, C. Song, Y. S. Hong, M. S. Kim, H. R. Cho, T. Kang, K. Shin, S. H. Choi, T. Hyeon and D. H. Kim, *Sci. Adv.*, 2017, **3**, 1–9.
178 H. Teymourian, A. Barfidokht and J. Wang, *Chem. Soc. Rev.*, 2020, **49**, 7671–7709.